Chem Soc Rev

Bridging the Gap between Academic Research and Industrial Development in Advanced All-Solid-State Lithium-Sulfur Batteries

Journal:	*Chemical Society Reviews*
Manuscript ID	CS-SYN-06-2023-000439.R2
Article Type:	Review Article
Date Submitted by the Author:	25-Mar-2024
Complete List of Authors:	Lee, Jieun; Argonne National Laboratory, Chemical Sciences and Engineering Division Zhao, Chen; Argonne National Laboratory, Chemical Sciences and Engineering Division Wang, Changhong; Eastern Institute for Advanced Study, College of Science Chen, Anna; Laurel Heights Secondary School Sun, Xueliang; Eastern Institute for Advanced Study, College of Science Amine, Khalil; Argonne National Laboratory Xu, Gui-Liang; Argonne National Laboratory, Chemical Sciences and Engineering Division

Chem Soc Rev

REVIEW ARTICLE

Bridging the Gap between Academic Research and Industrial Development in Advanced All-Solid-State Lithium-Sulfur Batteries

Received 00th January 20xx,
Accepted 00th January 20xx

DOI: 10.1039/x0xx00000x

Jieun Lee,[a] Chen Zhao,[a] Changhong Wang,[b] Anna Chen,[c] Xueliang Sun,[b] Khalil Amine*[a] and Gui-Liang Xu*[a]

The energy storage and vehicle industries are heavily investing in advancing all-solid-state batteries to overcome critical limitations in existing liquid electrolyte-based lithium-ion batteries, specifically focusing on mitigating fire hazards and improving energy density. All-solid-state lithium-sulfur batteries (ASSLSBs), featuring earth-abundant sulfur cathodes, high-capacity metallic lithium anodes, and non-flammable solid electrolytes, hold significant promise. Despite these appealing advantages, persistent challenges like sluggish sulfur redox kinetics, lithium metal failure, solid electrolyte degradation, and manufacturing complexities hinder their practical use. To facilitate the transition of these technologies to an industrial scale, bridging the gap between fundamental scientific research and applied R&D activities is crucial. Our review will address the inherent challenges in cell chemistries within ASSLSBs, explore advanced characterization techniques, and delve into innovative cell structure designs. Furthermore, we will provide an overview of the recent trends in R&D and investment activities from both academia and industry. Building on the fundamental understandings and significant progress that has been made thus far, our objective is to motivate the battery community to advance ASSLSBs in a practical direction and propel the industrialized process.

1. Introduction

The escalating global climate change crisis has prompted an urgent need to reduce carbon dioxide emissions by transitioning internal combustion engines to electric mobility systems, resulting in an ever-growing demand for advanced battery technologies capable of powering automotive and aviation applications. This uprising demand brought attention to significant concerns surrounding the energy density, safety, and supply chain risks associated with conventional rechargeable batteries, emphasizing the need for next-generation battery systems that can provide substantially improved energy density while maintaining economic viability. Among the various candidates, lithium-sulfur (Li-S) batteries, which utilize sulfur as the cathode material and lithium metal as the anode material, have emerged at the forefront of post lithium-ion batteries. The appeal of Li-S batteries lies in their high theoretical energy, with sulfur boasting 1,672 mAh g^{-1} and lithium reaching 3,860 mAh g^{-1}. As a result, Li-S batteries can achieve up to 600 Wh kg^{-1} of energy density (Fig. 1A).[1-6] Furthermore, the abundant availability and low cost of elemental sulfur contribute to the estimated minimum cost of the Li-S batteries, as low as 36 US$ kWh^{-1} (Fig. 1B), positioning them as a highly attractive choice among post lithium-ion battery systems.[7]

Significant advancements have been achieved in Li-S batteries, including the design of cathode structure and electrolyte additives (Fig. 2). However, despite these achievements, several challenges, such as low ionic and electronic conductivity of sulfur,[8] the dissolution of polysulfides and their shuttling,[9, 10] the substantial volume expansion/contraction of sulfur,[11] and the growth of dendritic Li metal, continue to impede the practical application of Li-S batteries.[12-14] To address these issues, there has been considerable attention given to the

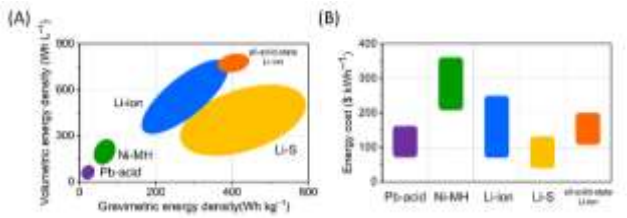

Fig. 1 (A) Comprehensive comparison illustrates the volumetric and gravimetric energy densities of different rechargeable batteries. (B) Energy cost comparison between different rechargeable batteries.

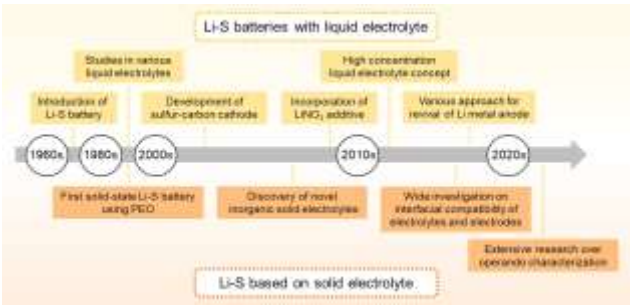

Fig. 2 Advancement of Li-S batteries with liquid and solid-state electrolytes.

[a] Chemical Sciences and Engineering Division, Argonne National Laboratory, 9700 S Cass Ave. Lemont, IL 60439, USA, E-mail: amine@anl.gov, xug@anl.gov
[b] Eastern Institute for Advanced Study, Eastern Institute of Technology, Ningbo, Zhejiang, 315200, P. R. China
[c] Laurel Heights Secondary School, 650 Laurelwood Dr, Waterloo, ON, Canada, N2V 2V1

development of all-solid-state Li-S batteries (ASSLSBs).[15] When comparing Li-S batteries utilizing different electrolyte types, it is crucial to note that the reaction mechanism of sulfur differs (Fig. 3). The overall sulfur redox process is represented as $S_x+2xLi^++2xe^-\rightleftharpoons xLi_2S$. In liquid and polymer electrolytes-based Li-S batteries, the conversion of elemental sulfur (S_8) follows a multi-phase transformation involving transitions between solid, liquid, and then back to solid states, exhibiting two voltage plateaus in the discharge voltage profile (Fig. 3A and 3B). Through a multi-step process, intermediate products, namely polysulfides (Li_2S_x, $6 \leq x \leq 8$) are formed. The polysulfides dissolve into the liquid or certain polymer electrolytes and subsequently undergo reduction, ultimately into solid lithium sulfide (Li_2S). Further characterization of the observed polysulfide shuttling in the polymer electrolyte will be covered in detail in Chapter 3.3. In contrast, inorganic solid electrolyte-based Li-S batteries undergo a single-phase solid-solid conversion, showing only one voltage plateau in the discharge voltage profile (Fig. 3C). In a single-step process, the elemental S is reduced to solid Li_2S in single-phase transformation due to the absence of a polysulfide solvating medium. The substitution of liquid electrolytes with solid-state electrolytes is expected to address many of the drawbacks associated with liquid electrolyte-based Li-S batteries, such as polysulfide shuttle effect and Li dendrite propagation.[16, 17] Moreover, the integration of solid-state electrolytes enhances safety from fire hazards, mainly originating from flammable organic solvents in liquid electrolytes.[18, 19]

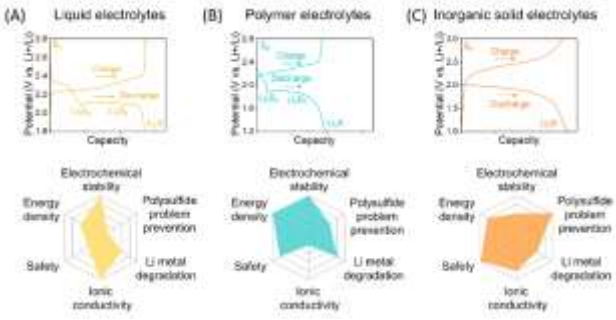

Fig. 3 Comparison of reaction mechanisms and properties between (A) liquid, (B) polymer, and (C) inorganic solid electrolytes-based Li-S batteries.

In pursuit of meeting commercial demands for the superhigh energy density of all-solid-state Li-S batteries, calculations were performed on their gravimetric energy density by varying the parameters of electrode components (Fig. 4). The gravimetric energy density of all-solid-state Li-S batteries, assuming 100% sulfur utilization, was calculated using various solid electrolytes, including polymer (polyethylene oxide, PEO), sulfide (Li_6PS_5Cl, LPSCl), oxide ($Li_7La_3Zr_2O_{12}$, LLZO), and halide (Li_3InCl_6) (Fig. 4A). Among these batteries, the cell using PEO exhibited the highest energy density, followed by LPSCl, Li_3InCl_6, and LLZO, at the same sulfur loading. This order of energy density is in inverse proportion to the density of each solid electrolyte: 1.2 g cm^{-3} (PEO), 1.64 g cm^{-3} (LPSCl), 2.59 g cm^{-3} (Li_3InCl_6), and 5.1 g cm^{-3} (LLZO). When utilizing the same solid electrolytes, the gravimetric energy density increased with the increase of sulfur loading. Besides, varying the N/P ratio of the cells showed that the gravimetric energy density decreased with an increasing N/P ratio (Fig. 4B). A smaller N/P ratio closer to 1 resulted in a higher energy density. Moreover, as the amount of sulfur increased (whether the sulfur content increased at the same loading or the sulfur loading increased at the same content within the composite), the gravimetric energy density of the cell also increased (Fig. 4C and

Jieun Lee

Jieun Lee is currently a postdoctoral researcher in the Chemical Sciences and Engineering Division at Argonne National Laboratory. She earned her bachelor (2016) and Ph.D. (2022) degree from Seoul National University. Her research interests focus on designing various electrode materials and fabrication technologies for all-solid-state batteries.

Guiliang Xu

Gui-Liang Xu is a chemist in the Chemical Sciences and Engineering Division at Argonne National Laboratory and holds an adjunct CASE scientist at the PME school of UChicago. He holds a bachelor (2009) and PhD (2014) degree from Xiamen University. With over a decade of research experience, his expertise lies in design and synthesis of multifunctional materials for energy storage, encompassing Li-ion, Na-ion, Li-S, and solid-state batteries. Also, he employs cutting-edge characterization techniques to understand the relationship between material structures and performance, providing insights and strategies to design and synthesize improved battery materials with enhanced energy density and safety features.

Khalil Amine

Khalil Amine holds the position of Argonne Distinguished Fellow and serves as the Manager of Advanced Battery Technology programs at Argonne National Laboratory. In this role, he oversees the research and development of advanced materials and battery systems for a wide range of applications including HEV, PHEV, EV, satellite, military, and medical uses. Additionally, he is a professor at UChicago and an adjunct professor at Stanford University. He is a board member of the committee on fuel economy of light duty vehicles at the National Research Council, Member of the National Academy of Inventors, the president of the International Lithium Battery Association (IMLB), chairmen of the International Automotive lithium battery (IALB), and ECS Fellow.

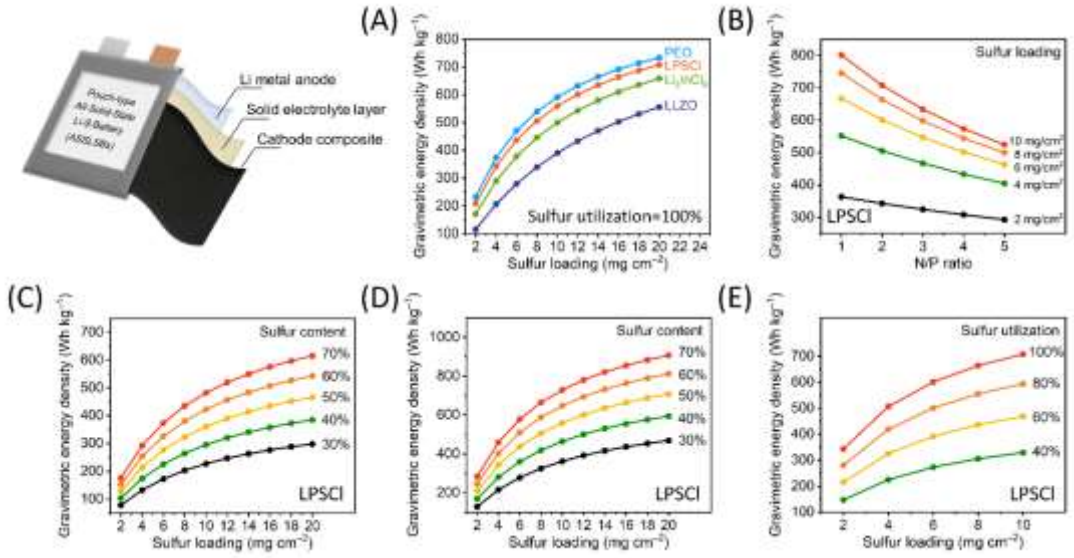

Fig. 4 (A) Calculated gravimetric energy density versus areal sulfur loading for all-solid-state Li–S pouch cells utilizing various solid electrolytes, including polymer (polyethylene oxide, PEO), sulfide (Li_6PS_5Cl, LPSCl), oxide ($Li_7La_3Zr_2O_{12}$, LLZO), and halide (Li_3InCl_6), assuming 100% sulfur utilization. (B) Calculated gravimetric energy density versus N/P ratio for all-solid-state Li–S pouch cell utilizing LPSCl as a solid electrolyte with various areal sulfur loadings, assuming 100% sulfur utilization. (C, D) Calculated gravimetric energy density versus sulfur loading for all-solid-state Li–S pouch cell utilizing LPSCl as a solid electrolyte with sulfur content from 30% to 70% within the composite cathode, assuming sulfur utilization of (C) 60% and (D) 100%. (E) Calculated gravimetric energy density versus areal sulfur loading for all-solid-state Li–S pouch cell utilizing LPSCl as solid electrolyte with sulfur utilization from 40% to 100%.

4D). Furthermore, when the sulfur loading and content were the same, higher sulfur utilization resulted in a higher gravimetric energy density (Fig. 4E). For instance, in the case of LPSCl-based Li-S batteries, if the sulfur utilization is only 60%, the sulfur loading should be higher than 15 mg cm^{-2} with a sulfur loading over 60% to achieve an energy density over 500 Wh kg^{-1} (Fig. 4C). Meanwhile, if the sulfur utilization can reach 100%, the sulfur loading of the cell can be as low as 8 mg cm^{-2} with a sulfur loading of 50% (Fig. 4D). Overall, to realize all-solid-state Li-S batteries with an energy density exceeding 500 Wh kg^{-1}, it is crucial to have a sulfur loading and utilization of at least 6 mg cm^{-2} and 80% or 4 mg cm^{-2} and 100% when utilizing LPSCl as a solid electrolyte. For the simulations, the composition of the cathode composite (sulfur:carbon:solid electrolyte) was set to 5:2:3 in weight ratio unless otherwise indicated, except for Fig. 4C and 4D. In all cases, the thickness of the solid electrolyte layer was 30 μm, and the N/P ratio was set to 2 unless indicated, except for Fig. 4B.

Extensive research efforts have been dedicated to the development of all-solid-state Li-S battery technology by both academia and industry, but it still faces significant challenges on the path towards commercialization. [20-23] Bridging the gap between basic research and applied development activities, often referred to as the "valley of death," remains a significant hurdle in transforming early-stage discoveries into mature and deployable technologies. It is crucial and urgent to provide a comprehensive and authoritative summary of the latest achievements from both academic research and industrial investigations to expedite the implementation of all-solid-state Li-S batteries. This review aims to offer a detailed overview of the most recent developments (since 2020) in all-solid-state Li-S batteries. Given the complexity and challenges involved in this system, the engagement of research students, professors, and scientists from diverse backgrounds in materials science, electrochemistry, chemistry, engineering, physics, and more is essential to addressing the fundamental barriers. Furthermore, the active participation of industry is critical to transform innovative discoveries into mature and deployable technologies. Within this review, our focus will be on the design of high-performing solid-state electrolytes, fundamental understanding of all-solid-state Li-S batteries, structural design of cathodes, anodes, and electrolytes, as well as insights into interfacial electro-chemo-mechanical issues under realistic operating conditions. Additionally, it will provide valuable experience and industrial perspectives on the development of solid-state electrolytes and cells towards the practical application of all-solid-state Li-S batteries.

2. Overview of solid-state electrolytes

Solid-state electrolytes have gained renown for their ability to mitigate the fire hazard risk associated with conventional liquid electrolytes. [24-26] Representative solid-state electrolytes can be categorized into polymer, inorganic, and their composite types (Table 1). Polymer electrolytes are soft, adhesive, and offer excellent processability, enabling excellent solid-solid contact and eliminating the need for stack pressure during operation. However, in polymer-based all-solid-state batteries, the dissolution of polysulfides within certain types of polymer matrices, along with their shuttling throughout the cell, presents significant obstacles. In addition, their low ionic conductivity restricts their functionality to high-temperature conditions. In contrast, inorganic solid electrolytes, including sulfide, oxide, and halide electrolytes, generally exhibit higher ionic conductivity. Given the low ionic conductivity of sulfur and lithium sulfide, it is essential to utilize solid electrolytes with significantly high ionic conductivity. Moreover, a higher ionic conductivity is always preferable. Additionally, due to the low electronic conductivity of sulfur, a significant amount of carbon is typically added to the

Table 1 Electrochemical, mechanical, and chemical properties of various solid-state electrolytes.

	Polymer	Composite	Inorganic solid electrolytes		
			Sulfide	Oxide	Halide
Ion Conductivity (S cm^{-1})	10^{-5}	10^{-4}	10^{-2}–10^{-4}	10^{-4}–10^{-5}	10^{-3}–10^{-5}
Electrochemical Stability Window (V)	0–4.5	0–6	1.5–2.5	0–3.5 (LLZO) 2–4 (LATP) 0–3 (Li_3OCl)	0.5–4 (Chloride) 0.5–3 (Bromide)
Processability	Good	Good	Good	Poor	Good
Mechanical Strength	Poor	Moderate	Moderate	Good	Moderate
Air Stability	Good	Good	Sensitive to H_2O	Mostly Good (LLZO sensitive to H_2O, CO_2)	Sensitive to H_2O

cathode composite in all-solid-state Li-S batteries. Given carbon's high surface area and low density, employing a low-density solid electrolyte would be more effective in establishing a continuous ion conduction pathway within the composite. In addition, solid electrolytes encounter challenges related to poor physical contact between particles, necessitating high external pressure during both fabrication and cell cycling. In certain cases, high-temperature sintering is required for oxide electrolytes. Issues of chemical and electrochemical instability pose significant obstacles for solid-state electrolytes. Fortunately, most solid-state electrolytes are compatible with sulfur cathodes, as their electrochemical stability window falls within the operational voltage range of sulfur (1.5─2.8 V). However, some solid reduction reactions may still occur. By employing solid-state electrolytes instead of their liquid counterparts, battery packs can achieve bipolar stacking, thereby reducing packaging costs, and further increasing their energy density. This trend bodes well for the future of solid-state electrolytes.

2.1 Polymers

Polymer electrolytes have attracted attention in research owing to their unique elasticity and favourable interfacial compatibility with the electrodes.[27, 28] Among the various polymers studied, polyethylene oxide (PEO) stands out as the most extensively investigated subject.[29] PEO has a wide electrochemical window of 0–4.5 V (vs. Li/Li^+), making it well-suited for use with lithium metal and sulfur cathodes in all-solid-state Li-S batteries. Additionally, its soft nature facilitates robust solid-solid contacts with electrode components, eliminating the need for stack pressure during cell cycling. Despite its prominence, PEO suffers from very low room-temperature ionic conductivity, measuring approximately 0.01 mS cm^{-1}, which severely limits its application to elevated temperatures above 60 ºC.[30, 31] To improve the ionic conductivity of PEO, researchers have primarily focused on reducing its crystallinity by incorporating heterogeneous polymers or forming composite electrolytes with inorganic particles to reduce the crystallinity of PEO and facilitate Li-ion conduction through the segmental motion of free polymer chains. One significant drawback of incorporating PEO in all-solid-state Li-S batteries is its susceptibility to the dissolution of polysulfides, which leads to the undesirable shuttle effect. Similar to liquid electrolytes, PEO solvates polysulfides, enabling the dissolved polysulfides to migrate from the cathode to the anode side. This shuttling causes the corrosion of lithium metal and the loss of sulfur, ultimately leading to rapid cell failure and further compromising its practical viability.[32, 33] These limitations have prompted researchers to explore the combination of multiple polymers together[34-36] or the implementation of cross-linking techniques.[34, 37, 38] These efforts aim to improve the mechanical strength of the electrolyte, minimizing lithium dendrite propagation and effectively trapping polysulfides to prevent shuttling, thereby enhancing overall stability and conductivity. On the other hand, novel polymer electrolytes different from PEO have been developed. However, many of the newly developed electrolytes require adding small amounts of liquid to achieve sufficient ionic conductivity. In practical terms, these are categorized as gel or quasi-solid-state electrolytes, thereby not strictly aligning with the definition of all-solid-state batteries. It is important to note that introducing liquid components may alter the rheological properties of electrodes and disrupt the bipolar stacking of cells. Despite these challenges, there are promising emerging approaches, such as polymer electrolytes utilizing salt-mediated crystal formation, which have gained popularity in recent studies.[39, 40] In some cases, polymer electrolytes are created through in situ polymerization within the cell using a precursor solution instead of pre-formed polymers. When the polymerization and subsequent drying process occur at temperatures above the boiling point of the solvent for a sufficient duration, the resulting electrolyte can be considered a solid-state electrolyte rather than a liquid-state or quasi-solid-state counterpart.

2.2 Composites

An alternative approach involves composite electrolytes, which are a combination of multiple solid-state electrolytes.[41, 42] The majority of reported composite electrolytes consist of polymer electrolytes filled with inorganic fillers. These fillers can be categorized as active fillers (e.g., sulfide electrolyte,[43-45] oxide electrolyte,[46-49] hydride electrolyte[50]) or passive fillers (e.g., In_2O_3,[41] Al_2O_3,[51] fullerene,[52] BN,[53] ceramic nanosheets,[54] MOF[55]) depending on whether the fillers conduct Li-ions or not. In composite polymer electrolytes, Li-ions can conduct through several pathways: along the polymer chains,[56] across the interfaces between the fillers and polymer,[57] or through the fillers.[58] Composite electrolytes with passive fillers primarily utilize the first two mechanisms, whereas those with active fillers take advantage of the Li-ion conducting properties of the active components. Incorporating fillers in polymer electrolytes offers significant benefits while retaining the advantageous characteristics of traditional polymer electrolytes, such as excellent processability. Firstly, it enhances the ionic conductivity and widens the electrochemical stability window of the composite electrolyte

compared to using polymer electrolytes alone. The fillers contribute to facilitating ion conduction and suppressing unwanted side reactions, leading to improved overall performance and safety. Secondly, the mechanical robustness of the composite electrolyte is greatly improved. The fillers reinforce the polymer matrix, making it more resistant to mechanical stress, while maintaining the desired deformability of the polymer electrolytes.

2.3 Sulfides

Among the inorganic solid electrolytes, sulfide electrolytes stand out as a highly promising candidate due to their exceptional room-temperature ionic conductivity that can reach up to 10 mS cm^{-1}.[59] These sulfide electrolytes are categorized into glass (e.g. Li_2S-P_2S_5),[60] glass-ceramics (e.g. Li_3PS_4, $Li_7P_3S_{11}$),[61] and crystalline solids (e.g. Argyrodite-type Li_6PS_5X (LPSX, X=Cl, Br, I, and their combination),[62, 63] LGPS-type $Li_{10}GeP_2S_{12}$[64]) based on their crystal structures. Early research predominantly focused on glasses and glass-ceramics. These often involved the mechanical synthesis of compounds like Li_2S and P_2S_5 alongside various sulfide, oxide, and halide compounds, followed by subsequent heat treatment. These initial efforts yielded a comparatively modest ionic conductivity of 0.1 mS cm^{-1}.[65] The late 2000s and following the 2010s marked an era of significant advancement in sulfide electrolytes by novel structures and synthesis techniques, including liquid-phase synthesis. Argyrodite structured sulfides gained popularity for their impressive ionic conductivity, utilization of cost-effective raw materials, and decent electrochemical stability in both oxidation and reduction.[66] Various LGPS-type sulfides attracted a surge of interest for their exceptionally high ionic conductivity, reaching as high as 25 mS cm^{-1},[67] but their application was hindered by instability against reduction when in contact with Li metal. Many of the sulfide electrolytes containing metallic or semi-metallic elements such as Sn, Si, and Ge suffer from the continuous growth of the conductive solid electrolyte interphase (SEI) at the Li−electrolyte interface. Another appealing advantage of sulfides lies in their ductile mechanical properties. Sulfides are soft enough to establish good interfaces between particles through cold-pressing alone, eliminating the need for additional high-temperature sintering. While stack pressure remains essential to maintain close particle-to-particle contacts throughout the charge and discharge cycles, the ease of processing significantly simplifies the manufacturing process. On the other hand, a persistent drawback of sulfide electrolytes is their susceptibility to moisture and polar solvents. When exposed to a humid environment, sulfides undergo structural deterioration, leading to a sharp reduction in ionic conductivity to significantly lower levels. Moreover, the oxidation of sulfide produces toxic H_2S gas, imposing additional constraints.[68] Another limitation pertains to their inherently narrow electrochemical stability window, typically confined to 1.5–2.5V. This restricts their compatibility with Li metal, high-voltage layered oxides, and even sulfur cathodes.[69] Nevertheless, intriguing exceptions have arisen under specific kinetically constrained conditions. Notably, some of the sulfide electrolytes, such as LPSCl, have demonstrated successful operation within an expanded electrochemical window spanning from 0 to 4.3V, showing decent electrochemical performance with high-nickel $LiNi_xMn_yCo_{1-x-y}O_2$ (known as NCM or NMC) cathodes and Li metal electrodes.[70, 71] Sulfides are highly appealing for use in all-solid-state Li-S batteries because their electrochemical stability window overlaps with the typical operation voltage of sulfur cathodes (1.5─2.8 V). This overlap eliminates concerns regarding poor electrochemical stability in sulfide-based all-solid-state Li-S batteries.

2.4 Oxides

Oxide electrolytes are an appealing choice for good chemical stability[72] Representative oxide crystals are NASICON (e.g. $Li_{1.3}Al_{0.3}Ti_{1.7}(PO_4)_3$ (LATP)),[73] LISCION (e.g. $Li_{2+2x}Zn_{1-x}GeO_4$),[74] garnet (e.g. $Li_7La_3Zr_2O_{12}$ (LLZO)),[75] perovskite (e.g. $Li_xLa_{2/3-x/3}TiO_3$ (LLTO))[76] and anti-perovskite (e.g. $Li_3O(Cl, Br)$)[77] structures. Unfortunately, the oxides generally exhibit inadequate room-temperature ionic conductivity around 0.1 mS cm^{-1}.[78] Moreover, their inherent mechanical rigidity results in insufficient solid-solid contact and remarkably high grain boundary resistance. Consequently, oxide electrolytes necessitate either high-temperature sintering processes[79] or the incorporation of liquid/polymer components to achieve effective interfaces.[80] However, since sulfur sublimes at much lower temperatures than the sintering temperatures of oxides, co-sintering oxide catholytes and sulfur together are not feasible. This necessitates the development of alternative cathode composite preparation methods. Besides the critical current density (CCD), the maximum current density before the cell suffers from short-circuiting due to Li dendrite penetration stands at a mere 0.05 mA cm^{-2} for oxides, while sulfides typically exhibit values higher than 0.4 mA cm^{-2}.[81] LLZO demonstrates an impressively wide electrochemical stability window spanning from 0 to 3.5 V. In contrast, LATP maintains stability only within the range of 2–4 V, owing to its diminished reductive stability stemming from the reduction of metallic Ti elements upon contact with Li metal. Conversely, Li_3OCl exhibits exceptional reductive stability, rendering it a suitable material against Li metal. However, its oxidative stability falls short, leading to an electrochemical stability window of 0–3 V.[82] Fortunately, many oxide electrolytes are recognized for their robust chemical stability.[83] Nevertheless, LLZO, a widely used oxide electrolyte, degrades to form LiOH and Li_2CO_3 upon exposure to H_2O and CO_2, and Li_3OCl is sensitive to moisture. Additionally, an interesting point to note is that anti-perovskites possess relatively lower melting points, approximately 280 ºC, facilitating melt-infiltration processing.[84]

2.5 Halides

Halide-based electrolytes, identified by the chemical formula Li_aMX_b (with X = F, Cl, Br, and I), encompassing diverse metal elements, have aroused notable attention due to their impressive room-temperature ionic conductivity, achieving around 1 mS cm^{-1}, coupled with commendable oxidation stability.[85] The landscape of halide electrolytes dates back to the 1970s, yet most of these initial formulations exhibited low room-temperature ionic conductivity, leading to limited interest in halides as electrolytes. However, a turning point was marked by the discovery of highly ion-conductive Li_3YX_6 (with X = Cl, Br) in 2018,[86] which catalyzed rapid advancements in its application to all-solid-state battery technology. Subsequently, an array of halide solid electrolytes, including Li_3ErCl_6,[87] Li_3ScCl_6,[88] and Li_3HoBr_6[89] emerged on the research horizon. Yet, the extensive reliance on rare earth metals for these formulations raised economic concerns, prompting research

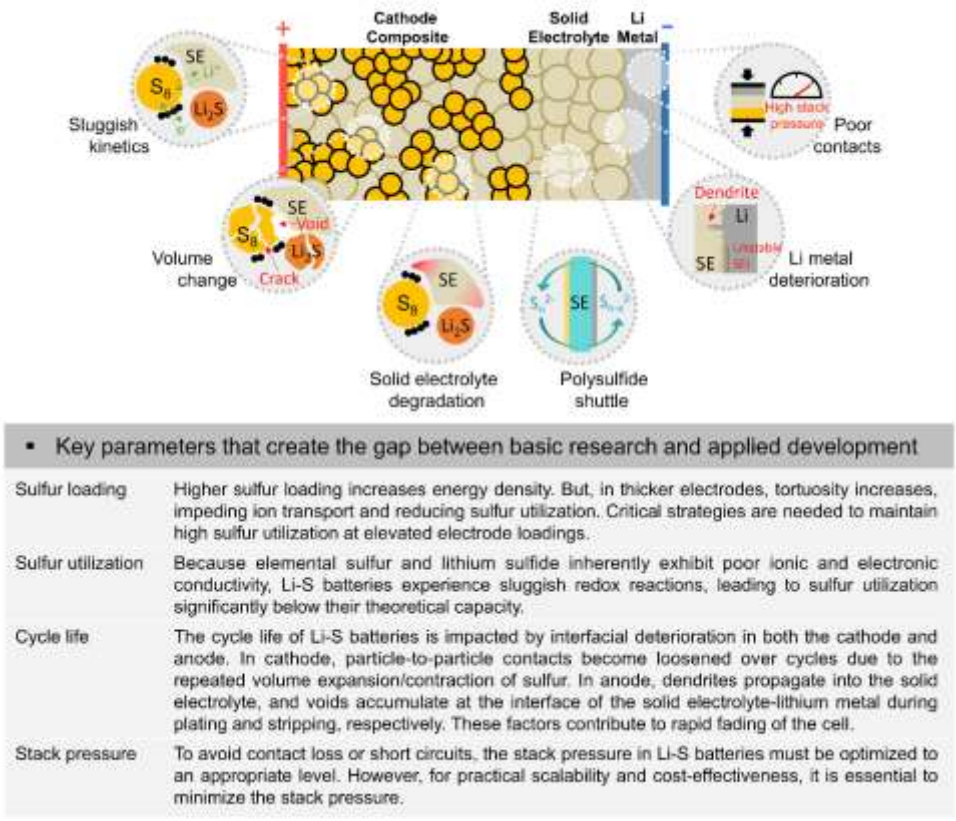

▪ Key parameters that create the gap between basic research and applied development	
Sulfur loading	Higher sulfur loading increases energy density. But, in thicker electrodes, tortuosity increases, impeding ion transport and reducing sulfur utilization. Critical strategies are needed to maintain high sulfur utilization at elevated electrode loadings.
Sulfur utilization	Because elemental sulfur and lithium sulfide inherently exhibit poor ionic and electronic conductivity, Li-S batteries experience sluggish redox reactions, leading to sulfur utilization significantly below their theoretical capacity.
Cycle life	The cycle life of Li-S batteries is impacted by interfacial deterioration in both the cathode and anode. In cathode, particle-to-particle contacts become loosened over cycles due to the repeated volume expansion/contraction of sulfur. In anode, dendrites propagate into the solid electrolyte, and voids accumulate at the interface of the solid electrolyte-lithium metal during plating and stripping, respectively. These factors contribute to rapid fading of the cell.
Stack pressure	To avoid contact loss or short circuits, the stack pressure in Li-S batteries must be optimized to an appropriate level. However, for practical scalability and cost-effectiveness, it is essential to minimize the stack pressure.

Fig. 5 Challenges in all-solid-state Li-S batteries.

endeavours aimed at developing cost-effective alternatives such as $Li_{2+x}Zr_{1-x}Fe_xCl_6$.[90] These materials are typically synthesized through ball-milling with subsequent annealing or water-mediated synthesis. Besides the shared advantages of high ionic conductivity and malleability akin to sulfides, one of the most distinct benefits of halides lies in their robust stability at elevated voltages. This feature enables their compatibility with cathode materials like $LiCoO_2$ (LCO) and high-nickel NCM without necessitating surface protective coatings, a challenge commonly encountered with sulfides. [91] However, a significant limitation of halide electrolytes pertains to their inadequate reductive stability, resulting in a restricted electrochemical stability range of 0.5–3 V.[92, 93] The insufficient stability at the anode necessitates the incorporation of at least one supplementary solid electrolyte partner when interfacing with lithium metal,[94] thereby presenting a subsequent challenge due to the disparity in solid electrolyte compatibility.[95] Similar to sulfide electrolytes, halide electrolytes are also susceptible to humidity-related issues.[96] However, it is noteworthy that these electrolytes form hydrated intermediate complexes that can be regenerated through heating, a more optimistic scenario compared to sulfides. Meanwhile, halides are soft enough to be easily processed. Yet, akin to other ceramic electrolytes, halide electrolytes require a certain degree of stack pressure during cycling to maintain favourable solid-solid contacts.

3. Challenges and advanced characterization of all-solid-state Li-S batteries

3.1 Fundamental challenges

While the potential advantages of all-solid-state Li-S batteries are promising, it is crucial to acknowledge the significant challenges that must be overcome in various material aspects, including design considerations of cathodes, anodes, and solid-state electrolyte layers, in addition to considerations regarding cell packaging and operational conditions (Fig. 5).[97, 98] Achieving high energy density batteries exceeding 500 Wh kg^{-1} requires targeting an areal energy density greater than 6 mAh cm^{-2}. This objective necessitates a high sulfur loading within the cathode, exceeding 4 mg cm^{-2} when assuming a sulfur utilization of 90%. Similar to other all-solid-state batteries, a thinner solid electrolyte layer is desirable for improved performance, with a thickness of around 30 μm considered suitable. Additionally, reducing the thickness of the lithium metal anode can further enhance energy density, with an N/P ratio close to 1 being preferable; ratios between 1.05 and 1.1 are acceptable. It is essential to optimize various key parameters to achieve the goals, with the primary objectives including achieving high capacity from a high sulfur loading cathode with high sulfur utilization for long cycle life. However, similar to liquid electrolyte-based Li-S batteries, limited sulfur utilization remains a critical concern in all-solid-state Li-S batteries owing to the inherently low Li-ion and electronic conductivities of sulfur and lithium sulfide. In contrast to layered oxide cathode materials such as $LiCoO_2$ and $LiNi_xCo_yMn_zO_2$, which exhibit considerably high ionic and electronic conductivity and may not require carbon additives in the cathode composite, sulfur cathodes necessitate a significant amount of carbon. This poses challenges for both processing and

electrochemical performance. The large surface area of carbons makes it difficult to process the cathode laminate using solution processing, as they absorb solvent extensively. Additionally, a large amount of carbon additive may facilitate detrimental solid electrolyte degradation. Thus, achieving high sulfur utilization without compromising fabrication conditions and cycle life is crucial. Another challenge lies in the substantial volume expansion and contraction of sulfur particles which can expand by as much as 80% during the transition from elemental S to Li_2S. This magnitude of volume change is much larger than that observed in other cathode materials, making it much more difficult to maintain close contact. This issue becomes notably pronounced when considering all-solid-state configurations. The absence of fluidic components exacerbates this issue by causing a complete rupture in the ionic pathway, subsequently leading to poor interfacial contact. On the other hand, the propagation of lithium dendrites poses another formidable challenge to the viability of all-solid-state Li-S batteries. Numerous strategies have been investigated to mitigate the issue of Li plating and stripping in all-solid-state batteries. These approaches encompass applying protective coatings to Li metal, incorporating electron-insulating compounds through doping or infusion into solid electrolyte materials and enhancing the mechanical strength of the solid-state electrolyte layer. However, an ideal solution has yet to be found. Precise calibration of cycling temperature and the delicate balance in stack pressure–demanding adequate pressure to minimize void formation during stripping while preventing excessive pressure that could lead to penetration of Li metal into the solid electrolyte during plating–emerge as critical factors. A noteworthy merit of inorganic solid electrolyte-based Li-S batteries is the alleviation of the polysulfide shuttling problem, as there is no medium for polysulfide generation and dissolution. Conversely, polymer electrolyte-based Li-S batteries encounter the same issue as their liquid electrolyte-based counterparts, which continues to be a significant drawback. Besides, certain solid electrolytes undergo either oxidative or reductive decomposition during charge and discharge cycles, warranting careful consideration.

3.2 Solid-state cell design for *in situ*/*operando* characterization

For a comprehensive understanding of the intricate electrochemical reaction mechanisms, battery researchers have employed a range of material characterization tools with cross-length-scale resolution. However, the inherent all-solid nature of ASSLSBs presents a series of challenges in post-cycling material analysis. Once meticulously assembled in cells, the electrode materials in all-solid-state Li-S batteries become interwoven, forming a cohesive unit that complicates easy disentanglement. This agglomeration not only hinders the extraction of individual components but also leads to cross-contamination among them, blurring the distinctive properties of the materials under scrutiny. Moreover, the fragile nature of these cells makes them susceptible to the formation of new cracks during disassembly, further complicating the distinction between cracks that emerged during cycling and those formed during the subsequent sample preparation for analysis.

To overcome these obstacles, *in situ* or *operando* characterization tools offering real-time information during battery cycling emerge as an appealing solution. A variety of *in situ*/*operando* characterization technologies, including optical, scanning probe, neutron, electron-based microscopic imaging, magnetic resonance, and *x*-ray

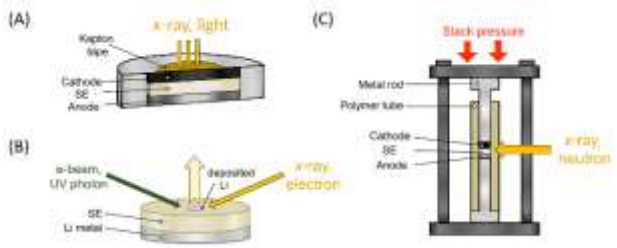

Fig. 6 Schematic illustration of various solid-state cells for in situ/operando characterization: (A) air-tight coin-cell, (B) virtual electrode cell, and (C) pressure-controlled cell.

spectroscopy, have been thoroughly explored in all-solid-state battery systems.[99] In the context of *in situ*/*operando analysis* within all-solid-state battery setups, especially those incorporating Li metal or air-sensitive solid electrolytes, specialized cell designs are essential to shield cell components from exposure to oxygen or moisture. The most straightforward and widely utilized approach for creating an air-tight environment involves the use of coin-cell casings with Kapton windows.[100] These cell casings are crafted with aligned openings on both the cell cases and spacers, with the openings on the cases covered by Kapton tape (Fig. 6A). This configuration enables the penetration of *x*-rays or light sources during cell operation while preserving an inert atmosphere within the cell. When examining components of the solid electrolyte interphase (SEI) or observing the nucleation and growth of metallic Li formations on solid electrolyte surfaces, the virtual electrode concept is often employed.[101, 102] This approach involves the application of e-beams or UV photons, which serve to supply negative or positive charge to the surface under analysis (Fig. 6B). In these cases, the surface of solid electrolytes is directly exposed to the ambient air, as any form of tape is removed to eliminate any hinderance to characterization. Therefore, the sample cells must be positioned within a humidity-controlled glovebox or, at the very least, within a controlled dry room environment during operation. Considering that inorganic solid electrolyte-based all-solid-state batteries inherently demand the application of external pressure during cycling, pressure-controlled cells are an essential prerequisite for achieving *in situ*/*operando* characterization (Fig. 6C).[103] Taking into account factors such as the beam size and the depth of energy source penetration, meticulous attention is given to the design of the thickness and diameter of the polymer tube encasing the samples for *operando* pressure-controlled cells. Furthermore, the material of this encasing tube should be thoughtfully chosen to prevent interference with the characterization process.

3.3 Sluggish/irreversible sulfur redox reaction

All-solid-state Li-S batteries encounter difficulties akin to those observed in liquid electrolyte-based Li-S batteries, primarily linked to the sluggish sulfur redox reaction. These challenges arise from the inherently poor Li-ion and electron conductivity of elemental sulfur and lithium sulfide.[104] The slow reaction kinetics of all-solid-state Li-S batteries have been elucidated through *in situ* imaging techniques. Bradbury et al. visualized the distribution of lithium within a composite sulfur cathode during cycling, employing *operando* neutron radiography and *in situ* neutron tomography. They observed the sulfur reduction propagating from the solid electrolyte layer toward the current collector side upon discharge, suggesting that the

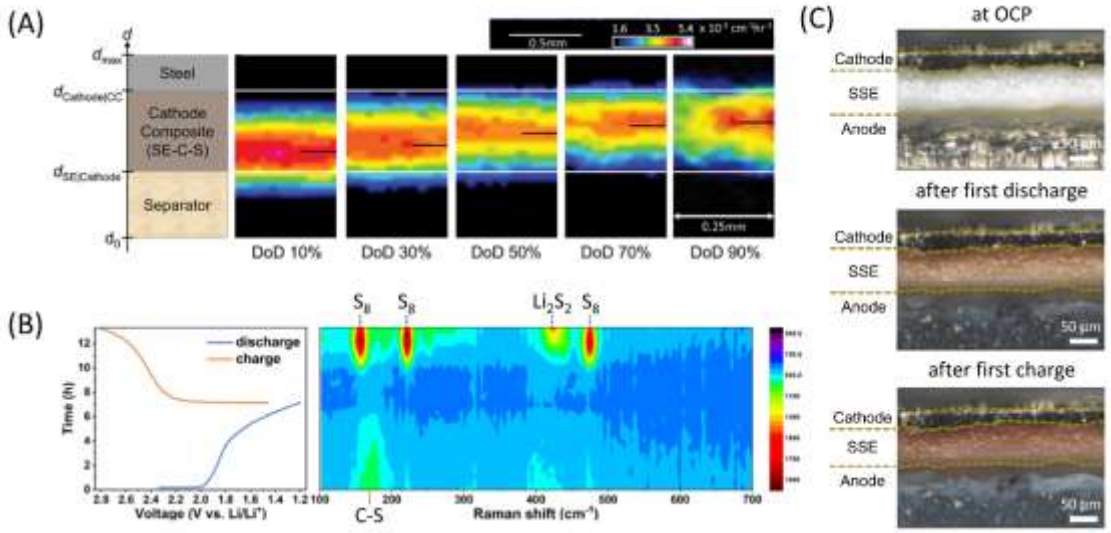

Fig. 7 (A) Dynamic evolution of lithium distribution in the all-solid-state Li-S batteries utilizing sulfide electrolytes (Li_6PS_5Cl) using *operando* neutron radiography as the degree of discharge (DoD) increases. Reproduced from ref. 105 with permission from Wiley-VCH Verlag GmbH & Co. KGaA, copyright 2023. (B) Time-voltage profile of the all-solid-state Li-S batteries utilizing $Li_{5.4}PS_{4.4}Cl_{1.6}$ sulfide electrolytes and the corresponding *operando* Raman intensity mapping during the cell testing. Reproduced from ref. 107 with permission from Wiley-VCH Verlag GmbH & Co. KGaA, copyright 2023. (C) *In situ* OM images of all-solid-state Li-S battery utilizing LiTFSI/PEO/LLZTO. Images captured at open circuit potential (OCP), and after the first discharge and charge. Reproduced from ref. 111 with permission from Elsevier, copyright 2021.

sluggish effective ion transport is the rate-limiting step (Fig. 7A).[105] Wang et al. demonstrated that Li-ion diffusion in Li_2S plays a dominant role in its reversibility in solid-state Li-S batteries through *in situ* transmission electron microscopy (TEM) observation.[106] These limited sulfur redox kinetics highlight the critical need to establish effective pathways for both Li-ion and electron transport.

While the discharge process of sulfur in liquid electrolyte-based Li-S batteries shows two voltage plateaus, indicative of a multi-phase sulfur redox mechanism, the discharge curve of inorganic solid electrolyte-based Li-S batteries displays a solitary plateau. This distinction implies that inorganic solid electrolyte-based Li-S batteries follow a different reaction mechanism. However, the details of this mechanism remained unclear and ambiguous (Fig. 3). Recently, Cao et al. proposed a reaction pathway wherein metastable Li_2S_2 was formed during the transition of S to Li_2S. Importantly, this reaction mechanism is characterized by the absence of polysulfide such as Li_2S_8, Li_2S_6 and Li_2S_4, as evidenced by *operando* Raman spectroscopy and *ex situ* synchrotron *x*-ray absorption spectroscopy (XAS) (Fig. 7B).[107] Meanwhile, Xiao et al. also utilized *ex situ* XAS to examine the discharge mechanism of sulfur cathode. Their findings disclose that sulfur underwent a stepwise reduction without the disproportionation reaction in sulfide electrolyte (Li_3PS_4)-based Li-S battery. Initially, it forms long-chain polysulfide (S_6^{2-}), followed by a subsequent reduction to midchain polysulfide (S_4^{2-}), short-chain polysulfide (S_2^{2-}), and ultimately into Li_2S.[108]

In inorganic solid electrolytes-based Li-S batteries, the lack of a medium for polysulfide dissolution makes them free from the polysulfide shuttle effect.[109] However, this challenge persists in polymer electrolyte-based Li-S batteries, similar to the liquid electrolyte-based ones. The generation of polysulfides, their dissolution into polymer electrolytes, migration to the Li anode, and the resulting deterioration of Li metal have been subject to extensive investigation including *in situ* optical microscopy (OM),[110] *in situ* atomic force microscopy (AFM),[111] *in situ* scanning electron microscopy (SEM), and *operando* ultraviolet–visible spectroscopy (UV-VIS).[112] Notably, Song et al. captured the change in the colour of polymer electrolytes, from bright-white to light-brown, a clear indicator of polysulfides dissolving into the electrolyte. (Fig. 7C).

3.4 Deterioration of solid-state electrolytes

Solid-state Li-S batteries face challenges associated with the irreversible chemo-mechanical failure caused by the deterioration of the solid electrolytes. The substantial volume expansion and contraction during the conversion of S into Li_2S exert significant internal stress on the surroundings, solid electrolytes, conductive agents, and current collectors. As a result, the integrity of particle-to-particle contacts within the composite cathode loosens, leading to the formation of voids and cracks. Unlike their liquid or polymer electrolyte counterparts, inorganic solid electrolyte-based Li-S batteries lack a flowable medium; thus, this absence exacerbates the impact of these morphological changes, resulting in severe capacity fading.[113-116] Besides, the oxidative and reductive degradation of sulfide solid electrolytes further detrimentally impacts the overall electrochemical performance.[117] Owing to the overlapping voltage ranges where sulfide electrolyte decomposition and sulfur redox

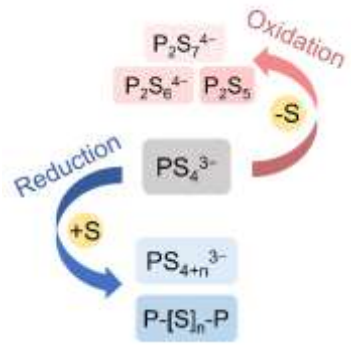

Fig. 8 Redox reaction of PS_4^{3-} thiophosphate unit of sulfides within sulfur charge/discharge voltage window.

occur, polysulfidophosphates (–P–S_n–P–) are formed and disappear in a reversible manner as a result of the reaction between PS_4^{3-} thiophosphate unit of sulfides and sulfur during the charge and discharge of sulfur (Fig. 8).[118] A positive aspect is that this reversible reaction of solid electrolytes occasionally contributes supplementary capacity to the sulfur redox capacity.[119-122] Nonetheless, prolonged cycles of solid electrolyte oxidation and reduction could deteriorate its effective ionic conductivity, ultimately leading to poor cycling performance over time.[123] Commonly, the decomposition of solid electrolytes is analyzed through *x*-ray diffraction (XRD), *x*-ray photoelectron spectroscopy (XPS), and Raman spectroscopy analysis after battery cycling. Additionally, dynamic electrochemical mass spectrometry (DEMS) provides real-time detection of gas evolution resulting from the degradation process in cell operation.[124]

3.5 Lithium degradation

The challenge of lithium dendrite propagation persists within the realm of all-solid-state batteries.[125] Numerous microscopic imaging tools have captured the propagation of lithium dendrites within solid electrolytes, a phenomenon directly linked to short circuit failures.[126-128] Interestingly, Liang et al. examined the accumulation of dead Li in sulfide solid electrolytes using *operando* nuclear magnetic resonance spectroscopy (NMR) in a recent study (Fig. 9A).[129] In polymer electrolyte-based lithium metal batteries, the penetration of lithium dendrites into polymer electrolytes arises from the low mechanical strength of the polymers.[130] In contrast, despite their considerably higher yield strength, the inorganic solid electrolyte-based lithium metal batteries remain susceptible to dendrite penetration. Various theories have been suggested to elucidate this phenomenon. For instance, one theory suggests that lithium tends to propagate along surface defects present on solid electrolyte grains.[131] Additionally, the inadequately low electronic conductivity of solid electrolytes can induce the reduction of lithium ions to metal.[132] Furthermore, during the deposition of lithium metal, cracks are formed and propagate, providing pathways for the propagation of dendrites. Ning et al. utilized *in situ x*-ray computed tomography (XCT) to demonstrate that lithium plating induces cracks first, followed by the growth of lithium dendrites through these cracks (Fig. 9B).[133] The growth of lithium dendrite within ceramic electrolytes ultimately leads to short circuits or, at the very least, soft shorting.[134]

The interphase formed between solid electrolytes and Li metal can also contribute to chemomechanical failure. This phenomenon becomes particularly pronounced when ceramic electrolytes containing metallic or semi-metallic elements (such as Ti, Ge, Sn, and Si) contact with Li metal. In these scenarios, the interphase presents mixed ionic-electronic conductor (MIEC) characteristics that continue to expand over time. The expansion of this interphase induces fractures within the material, causing an increase in interfacial impedances.[135]

Another noteworthy factor in the failure of all-solid-state lithium metal batteries is the development of voids at the interface between the solid electrolyte and the lithium metal layer during the stripping process.[136] Voids are formed when lithium is removed more rapidly than it is replenished. Over successive cycles, these voids accumulate, leading to an elevation in the local current density. Ultimately, this locally intensified current density drives the formation of dendrites during the electroplating process, resulting in short circuits, and eventual cell breakdown.[137, 138] Through the application of XCT, Lewis et al. observed the generation of voids during the process of lithium stripping in sulfide electrolyte-based symmetric cells (Fig. 9C). This contact loss has been recognized as the primary cause of cell failure in the case of solid electrolytes with MIEC-type interphase when short circuits are absent.[139]

3.6 Stack pressure

The operation of all-solid-state batteries becomes more intricate when considering the influence of external stack pressure (Fig. 10). In the context of the composite cathode, these batteries require significant external pressure during cycling.[140, 141] Throughout the charge/discharge process, the active materials undergo repeated expansion and contraction, often leading to the disconnection of

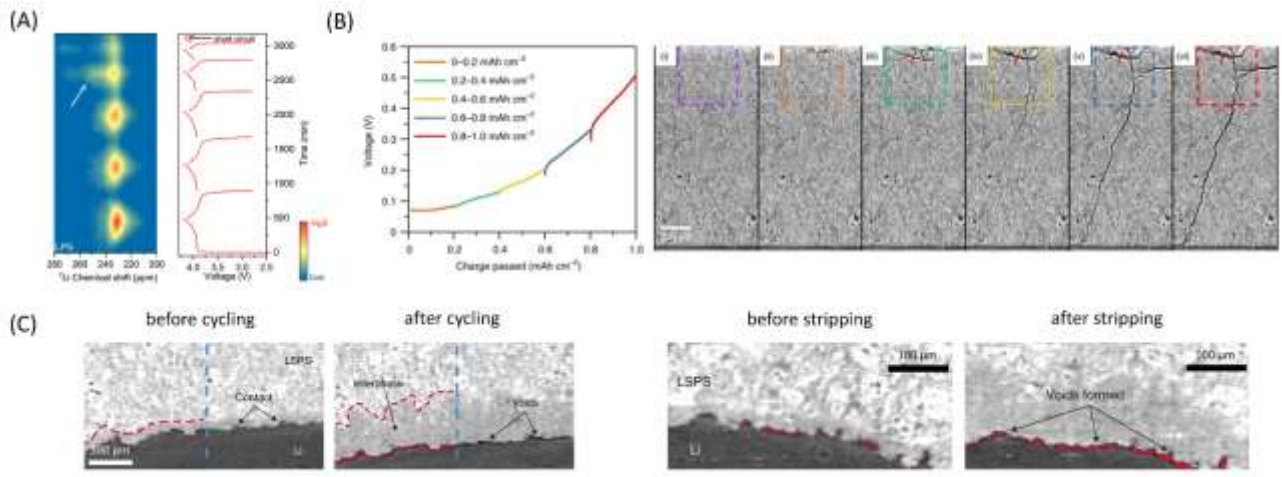

Fig. 9 (A) Contour plot of *operando* ^{7}Li NMR spectra and the corresponding charge/discharge voltage profiles of an anode-free battery employing $Li_7P_3S_{11}$ (LPS). Reproduced from ref. 129 with permission from Nature Publishing Group, copyright 2023. (B) *In situ* phase-contrast XCT virtual cross-sectional images captured during plating of a Li|Li_6PS_5Cl|Li cell. Reproduced from ref. 133 with permission from Nature Publishing Group, copyright 2021. (C) *Operando x*-ray tomography cross-sectional images of a Li|$Li_{10}SnP_2S_{12}$|Li cell (left) before and after cycling, and (right) before and after stripping. Reproduced from ref. 139 with permission from Nature Publishing Group, copyright 2021.

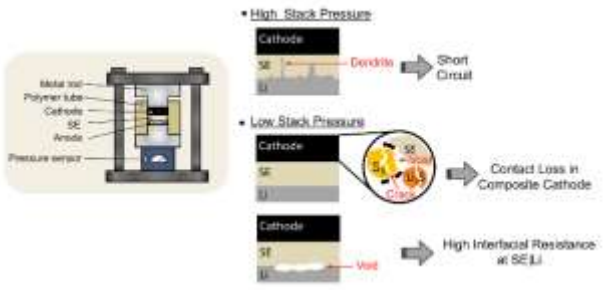

Fig. 10 Stack pressure considerations in various aspects of all-solid-state batteries.

electrode particles from each other and the formation of cracks and voids. To ensure close contact and minimize interface resistance, it becomes essential to apply external stack pressure. However, when dealing with the lithium metal anode, excessively high stack pressure can result in the unwanted penetration of metallic lithium into the solid electrolyte layer, potentially causing short circuits.[142] Conversely, if too low stack pressure is applied, the creep-induced deformation of lithium metal fails to replenish the vacant sites where lithium is stripped away, leading to numerous voids formed at the solid electrolyte/Li metal interface and an increase in interfacial resistance.[143, 144] Therefore, it is essential to apply the appropriate pressure to establish a robust solid electrolyte/Li metal interface. Nevertheless, for the practical scalability of batteries, applying significant stack pressure may not be feasible. Hence, there is a need to reduce stack pressure to the lowest possible level while considering technological and cost-effectiveness factors.[145, 146] *Operando* pressure monitoring has been thoroughly studied to examine volume fluctuations, corresponding changes in internal stresses, and cell pressure during battery operation.[147, 148] To measure these differences, a pressure sensor is typically inserted into the stacked cell housing.

4. Strategies to improve performance

In this section, the state-of-the-art technologies for fabricating all-solid-state Li-S batteries are explored (Table 2). The primary focus here is placed on the novel material designs and unique processing strategies of each electrode component, namely solid electrolytes, cathodes, anodes, and binders. These aspects, tailored to the requirements of all-solid-state batteries and distinguished from their liquid-based counterparts, are the central focus of this exploration.

4.1 Solid-state electrolytes

Elevating the ionic conductivity of solid-state electrolytes stands as a fundamental and widely adopted strategy for enhancing the electrochemical performance of all-solid-state Li-S batteries. The improvement in ionic conductivity directly influences both sulfur utilization within the cathode composite and Li-ion transport in the solid electrolyte layers. One common strategy to enhance the ionic conductivity is doping, or the substitution of heteroatoms within the lattice of inorganic solid electrolytes.[167-172] When foreign ions with varying charges or sizes are introduced into the solid electrolyte structure, they generate vacancies and expand ion transport channels, thereby facilitating the more facile conduction of Li-ions through these pathways. Moreover, the addition of doping compounds during synthesis serves to restrict the formation of low-conductivity polyhedral units, thus promoting the synthesis of highly ion-conductive phases.[173] This, in return, results in a significant increase

Table 2 A summary of the electrochemical performance data from the latest research papers on all-solid-state Li-S batteries.

Cathode	Solid electrolyte	Anode	Active material loading in cathode (mg cm^{-2})	Current density (mA cm^{-2})	Initial areal capacity (mAh cm^{-2})	Capacity retention	Temp. (ºC)	Ref.
Li_2S	$80Li_2S{\cdot}20P_2S_5$	Li	0.37 (Li_2S)	0.13	0.37	79.6%@100cyc	60	149
S	$65Li_{1.6}PS_2{\cdot}35LiI$	Li-In	4.8 (S)	8.0	6.4	91%@100 cyc	45	150
C@S	PEO/LLZTO/$Mg(TFSI)_2$	Li	0.5 (S)	0.4	0.17	94.1%@300cyc	60	151
KB@S	$Li_3PS_4{\cdot}2LiBH_4$	Li-In	2.57 (S)	2.15	2.6	77.5%@800 cyc	60	152
$Li_2S/Li_3PO_4/Li_2SO_4$	Li_3PS_4	Li-In	10 (Li_2S)	1.17	8.5	82.4%@100 cyc	25	153
rGO@S	$Li_{10}GeP_2S_{12}$	Li	0.4 (S)	0.67	0.37	89.2 %@750 cyc	60	154
KB@S	Li_3PS_4	Li-In	1.5 (S)	0.25	2.6	84.5% @100cyc	60	155
C-novel@S	Li_3PS_4	Li-In	2.6 (S)	1.3	3.12	91.7%@400cyc	25	156
Co@AB/S	Li_6PS_5Cl	Li-In	4.5 (S)	2.2	5.1	59.5%@300cyc	60	157
$Li_2S/LiVS_2$	$Li_{5.5}PS_{4.5}Cl_{1.5}$	Li-In	2 (Li_2S+$LiVS_2$)	1	0.95	77%@100cyc	25	158
Li_2S/AQT	PEO/LiTFSI	Li	0.7 (Li_2S)	0.08	0.8	88%@20cyc	60	159
MoS_2@CNT@S	Li_6PS_5Cl	Li-In	4 (S)	1	5.1	63.9%@250cyc	30	160
CMK-3@S	PEO/LiTFSI	Li	0.6 (S)	0.1	0.44	70.3%@400cyc	35	161
AB@S	$Li_{9.54}Si_{1.74}P_{1.44}S_{11.7}Cl_{0.3}$	Ag-C@Li_5B_4	1.3 (S)	0.42	1.7	82%@60cyc	60	162
KB@S	$Li_{10}GeP_2S_{12}$	LiI@Li	0.45 (S)	0.2	0.59	80.6%@150cyc	25	163
BC@S	PEO/PGA/LiTFSI/Py_{13}TFSI	Li	1.5 (S)	0.5	0.9	89%@100cyc	50	164
C@S	$Li_{10}GeP_2S_{12}$	Li-In	1.3 (S)	0.21	1.3	95.3%@30cyc	25	165
C@S	Li_6PS_5Cl	Li-In	2 (S)	0.3	3.2	65%@400cyc	25	166

in the ionic conductivity of the sulfide electrolyte. Furthermore, research has shown that the adjustment of the P/S ratio to a higher value in lithium phosphorus sulfide electrolytes effectively enhances ionic conductivity, consequently yielding superior rate performance.[150] To ensure the presence of sufficient Li-ion pathways between sulfur active materials in high-sulfur content cathodes, Wang et al. suggested employing solid electrolytes with low density. A low-density solid electrolyte enabled sulfur cathodes with a higher proportion of solid electrolyte volume, resulting in a more uniform cathode composite and facilitating high sulfur utilization (Fig. 11A).[152] In alternative approaches, achieving close contact between the electrode components was often accomplished through the *in situ* synthesis of sulfide electrolytes onto the surface of the active material (Fig. 11B).[174, 175] On the one hand, broadening the electrochemical stability of solid electrolytes is a crucial aspect of their design. In this context, Hakari et al. reported that substituting conventional sulfide catholytes with lithium oxyacid salts, such as Li_3PO_4 and Li_2SO_4, enhanced the oxidation stability of the Li_2S cathodes (Fig. 11C).[153]

In polymer or composite electrolyte-based Li-S batteries, substantial efforts have been directed toward mitigating polysulfide shuttle and lithium dendrite issues. Functional ionic salt additives were introduced to precipitate polysulfides on the cathode, blocking their shuttling. Simultaneously, these additives contribute to building a favourable SEI on the lithium metal anode, suppressing dendrite formation.[151, 176] Moreover, novel anion structures were designed to increase chemical compatibility with polysulfides during cycling and induce facile decomposition to form ionic conductive SEI components.[177]

4.2 Cathode

The cathode design is crucial for optimizing the cell performance of all-solid-state Li-S batteries. Given the inherent ionic and electronic insulating nature of both sulfur and lithium sulfide, it becomes imperative to integrate a substantial amount of conductive agents, predominantly carbon, along with solid electrolytes and active materials. Therefore, ensuring a homogeneous mixture of components in the composite cathode to increase sulfur utilization in the redox reactions is a critical consideration.

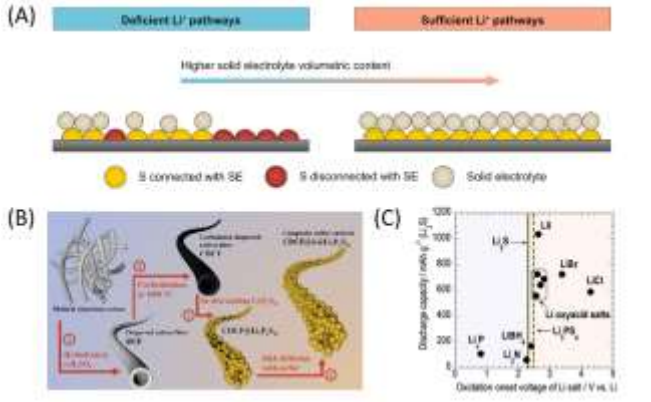

Fig. 11 (A) Schematic illustration depicting enhanced Li-ion pathways with increased solid electrolyte volume content (decreased density) in the sulfur cathode. Reproduced from ref. 152 with permission from Nature Publishing Group, copyright 2023. (B) Schematic illustration detailing the preparation of a sulfur cathode composite by *in situ* coating of sulfide electrolyte on carbon fiber followed by sulfur infusion. Reproduced from ref. 175 with permission from Elsevier, copyright 2020. (C) Relationship between the discharge capacities in all-solid-state Li_2S batteries with cathode composites incorporating Li salts and the oxidation onset voltages of Li salts. Reproduced from ref. 153 with permission from Wiley-VCH Verlag GmbH & Co. KGaA, copyright 2021.

To establish a well-connected triphase encompassing sulfur active material, carbon, and solid electrolytes, efforts have been directed towards reducing the dimensions of both active material and solid electrolyte particles[149, 178] or minimizing the crystallinity of sulfur by preparing it in an amorphous state.[154] The predominant strategy employed to reduce the size and crystallinity of sulfur while enhancing electronic conductivity is the incorporation of sulfur into a carbon structure. In a recent paper, a novel approach has emerged, replacing traditional solid electrolytes and carbon with lithium halide as a dopant to increase the ionic conductivity of lithium sulfide. Additionally, MoS_2 was utilized as a high electronic conductivity additive in this design.[179]

Additionally, recent studies have explored the integration of various redox mediators into the cathode to further improve the sulfur redox reaction and minimize polysulfide diffusion. Alongside advancements in material properties, various compositing processes have been investigated, aiming not only for superior battery performance but also enhanced productivity. A cutting-edge technology has been developed to repair the damaged interfaces that occurred during cycling in all-solid-state Li-S batteries. This innovation involves incorporating iodine into sulfur, lowering the melting point so that by heating the cells to 100 °C, the integrity of the interfaces can be restored, improving the overall performance and longevity of the battery.[180]

4.2.1 Sulfur-impregnated carbon

Various methods have been employed to create sulfur-impregnated carbon cathodes, including mechanical milling,[181] solution infusion,[182, 183] melt infusion,[184] and vapor deposition.[155] Mechanical milling is executed by mixing the powder mixture using a planetary ball-mill apparatus. In the solution infusion method, sulfur is reduced from a sulfur-amine complex precursor solution. The melt infusion method involves melting sulfur in a sealed vessel at approximately 150 °C, while vapor deposition encompasses the sublime of sulfur at temperatures higher than 300 °C. Among these techniques, vapor deposition stands out as the most effective method for fully amorphasizing sulfur, although melt infusion and mechanical milling are somewhat less efficient (Fig. 12A). However, it is noteworthy that the more effective methods tend to be more complex and less cost-effective.

The sulfur loading level in the sulfur-impregnated carbon cathode and its electronic conductivity depends on the type of carbon used. Therefore, various carbon materials have been explored to understand and optimize these properties. To increase sulfur loading, it is preferable to use interconnected meso/microporous carbons with high porosity and a larger surface area, allowing for a larger volume to accommodate sulfur content (Fig. 12B).[156, 185-187] One-dimensional (1D) carbons, such as single or multi-walled carbon nanotubes (CNTs) or vapor grown carbon fibers (VGCFs), are often used to establish continuous paths for excellent electron conductivity.[188, 189, 190] The fabrication of continuous carbon fiber frequently employs the electrospinning method. Wang et al. fabricated lithium lanthanum titanium oxide (LLTO)/C nanofibers by electrospinning a mixture of LLTO precursor and polyacrylonitrile, followed by a subsequent calcination process.[191] Afterwards, sulfur nanoparticles were

introduced onto the LLTO/C nanofibers using a straightforward dip-loading method. This led to the formation of ionic/electronic conductive double-phase interfaces of sulfur-LLTO/C, demonstrating enhanced sulfur utilization.

Beyond carbon structural design, the incorporation of heteroatoms and nanosized additives onto the carbon surface has become a widely recognized strategy for enhancing sulfur redox kinetics (Fig. 12C).[192, 193] Single-atom catalysts, such as nickel and cobalt, which exhibit a strong chemical affinity with sulfur, accelerated the sulfur conversion and prevented the agglomeration of sulfur particles.[157] In polymer electrolyte-based Li-S batteries, single-atom electrocatalysis has also demonstrated its efficacy in minimizing the formation of dead lithium polysulfides as well.[194]

4.2.2 Redox mediator

Redox mediators participate in the conversion reaction of sulfur, reducing the activation energy. They encompass a broad range of compounds, including metal sulfides and organic molecules. Metal sulphides such as VS_2,[195] Y_2S_3,[196] Al_2S_3,[197] FeS_2,[198], and CuS[199] have been discovered in sulfide-based Li-S batteries due to their compatibility with both sulfur and sulfide electrolytes. These metal sulfides contribute to the reversible capacity of cells in addition to sulfur. Unlike the poor ionic/electronic conductivity of sulfur and Li_2S, many metal sulfides exhibit mixed ionic-electronic conducting conductivity, serving as dual-charge carrier transport channels. Additionally, they also play a role in mitigating the severe volume change of sulfur during cycling. In its role as a mediator, VS_2 possesses a redox potential slightly higher than that of the Li_2S active material, enabling efficient engagement in the sulfur redox reaction (Fig. 12D). If TiS_2, another popular metal sulfide compound, were

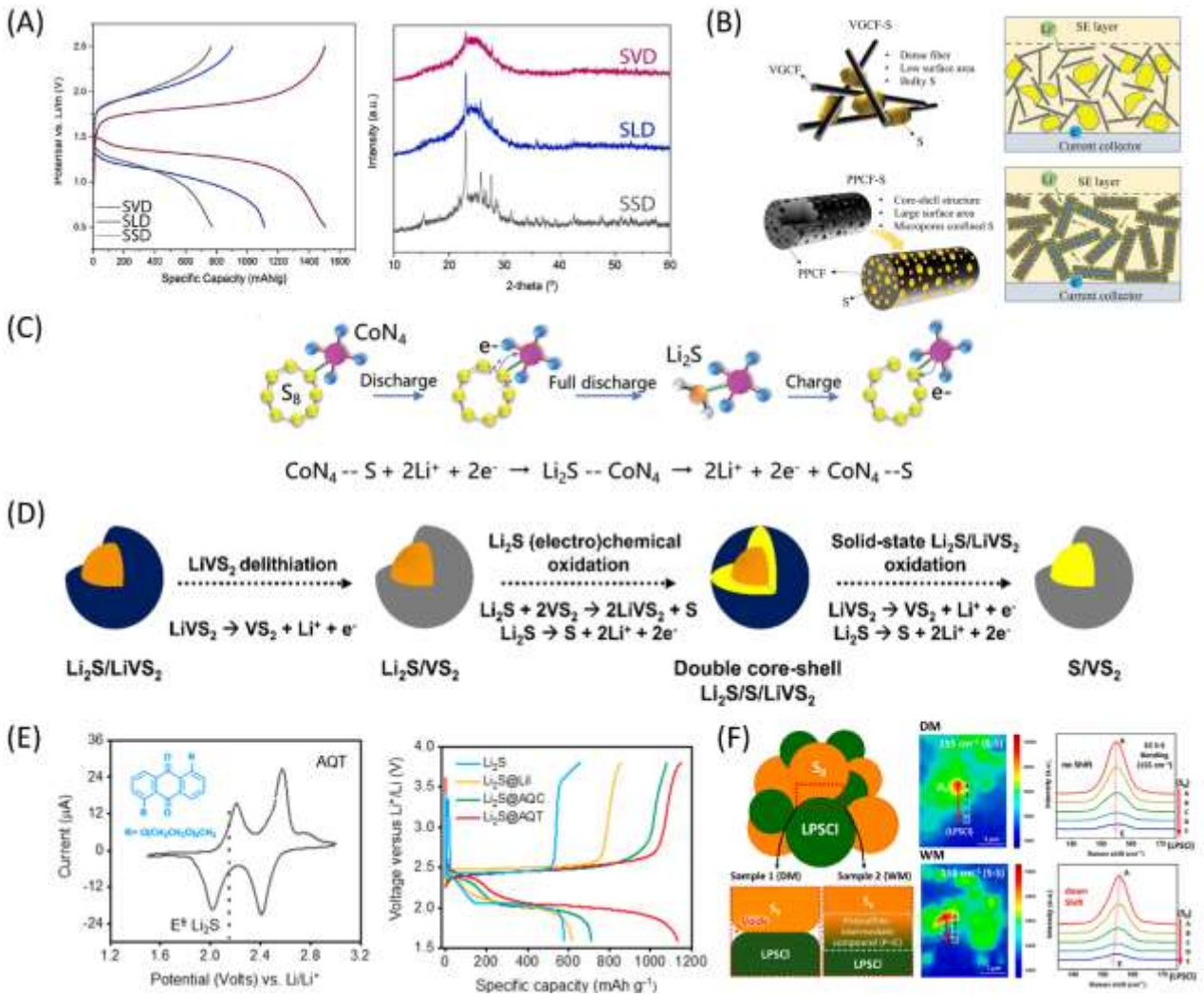

Fig. 12 (A) XRD pattern for sulfur–carbon composites prepared *via* solid deposition (SSD), liquid deposition (SLD), and vapor deposition (SVD) methods (left) and third charge/discharge voltage profiles of samples prepared using various methods. (right). Reproduced from ref. 155 with permission from American Chemical Society, copyright 2021. (B) Schematic illustration of the structural influence of carbon additives on conducting pathways within the cathode. Reproduced from ref. 188 with permission from Wiley-VCH Verlag GmbH & Co. KGaA, copyright 2021. (C) Schematic illustration of the catalytic mechanism involving single-atom catalysts decorated on carbon additives in sulfur redox kinetics. Reproduced from ref. 157 with permission from Wiley-VCH Verlag GmbH & Co. KGaA, copyright 2023. (D) Schematic illustration of the Li_2S oxidation reaction mechanism mediated by VS_2. Reproduced from ref. 158 with permission from Royal Society of Chemistry, Copyright 2023. (E) Cyclic voltammetry profile of the quinone-based redox mediator (AQT) (left) and charge/discharge curves of Li_2S cathodes using various redox mediators during the first activation cycle (right). Reproduced from ref. 159 with permission from American Chemical Society, copyright 2021. (F) Schematic illustration (left), Raman mapping (middle) and spectra (right) of the interfaces formed between sulfur and sulfide electrolytes depending on the mixing method–whether dry or wet. Reproduced from ref. 160 with permission from American Chemical Society, copyright 2023.

utilized instead, it would not be a feasible mechanism due to its lower potential relative to that of Li_2S.[158]

In polymer electrolyte-based Li-S batteries, organic molecules were studied as potential redox mediators. Among these, the anthraquinone-type redox mediator met two essential criteria: solubility in PEO polymer electrolyte and a redox potential slightly higher than that of Li_2S (Fig. 12E).[159] Notably, it effectively reduces the energy barrier for Li_2S oxidation, demonstrating its functionality in enhancing cycling stability.

4.2.3 Fabrication strategies

Ball milling is a basic method for processing composite cathodes. When utilizing a planetary ball-milling apparatus, particle distribution becomes more homogeneous compared to mortar mixing. Multi-step ball-milling, incorporating different speeds, further improves the interfacial area between sulfur and solid electrolytes.[200] Iwao et al. employed the hot-melt kneading technique for the scalable processing of sulfur/carbon composites. In this process, powder was fed into a twin-screw kneader, undergoing exposure to controlled heat and shear forces. The heater temperature was adjusted to selectively melt sulfur, allowing carbon to be embedded within the sulfur matrix, thereby improving the electrochemical performance.[201]

Solution processing stands as a commonly adopted strategy for achieving intimate solid-solid interfaces. In this method, solid electrolytes were either synthesized *in situ* from precursors through a liquid-phase process, forming a thin coating on the surfaces of active materials and carbon additives,[174] or pre-synthesized solid electrolytes were prepared by dissolution-precipitation. In another approach, both solid electrolytes and sulfur were dissolved in a solution and infiltrated into porous carbon structures.[202] Meanwhile, Kim et al. pointed out the importance of solvent selection in the solution processing of sulfur cathode.[160] Wet milling of cathode composites with a weakly polar solvent induced a chemical reaction between elemental sulfur and sulfide solid electrolytes. As a result, a polysulfido-intermediate phase formed at the interfaces, establishing excellent solid-solid contacts (Fig. 12F).

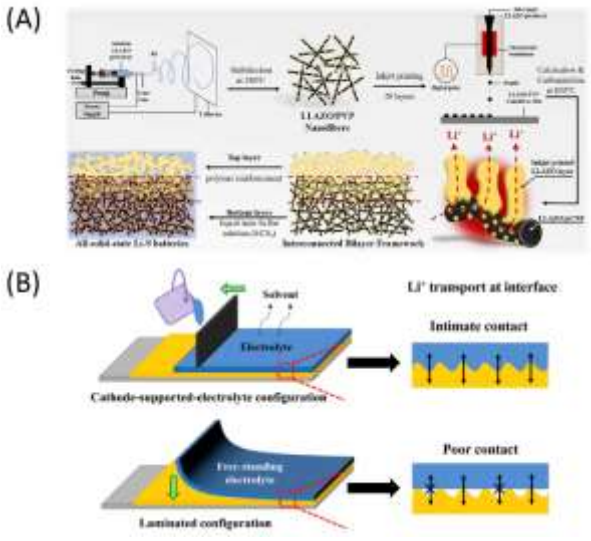

Fig. 13 (A) Schematic illustration of the fabrication process for the interconnected bilayer framework of LLAZO-based Li-S batteries. Reproduced from ref. 203 with permission from Elsevier, copyright 2022. (B) Schematic illustration of the fabrication process of the cathode-supported-electrolyte and free-standing electrolyte type cell configurations. Reproduced from ref. 204 with permission from American Chemical Society, copyright 2020.

4.3 Interface modification

Beyond fabrication methods, researchers have determined cell layer configurations to enhance Li-ion conduction, exploring double-layer fabrication techniques distinct from traditional batteries with separated layer compositions. The focus has been on creating interconnected cathode-electrolyte bilayers, with strategies categorized into two types. The first type involved a design where the oxide electrolyte framework interconnects the cathode matrix and electrolyte layer (Fig. 13A).[203] Yan et al. achieved it by electrospinning $Li_7La_3Zr_2O_{12}$ (LLZO) precursors with polyvinylpyrrolidone (PVP), followed by inkjet-printing the LLZO precursor onto the top of the first layer. Subsequent calcination resulted in the decomposition of the oxide electrolyte precursor into the garnet phase, while PVP was carbonized. This process resulted in the cathode consisting of a continuous bilayer of LLZO@CNF filled with sulfur at the bottom and an LLZO layer on top. The second type involved a cathode-supported electrolyte approach (Fig. 13B).[204] Here, a sulfur electrode slurry was blade-cast onto the current collector, fully dried, and then a PEO solution was directly cast onto the electrode layer. In both continuous cathode-electrolyte double-layer fabrication approaches, the two layers exhibited intimate interfacial contacts, ensuring they were not easily peeled off from each other. Moreover, these configurations facilitated the construction of continuous ionic conduction pathways within the cell, contributing to enhanced overall performance.

In polymer electrolyte-based Li-S batteries, a popular strategy to address the challenge of polysulfide shuttling involves the insertion of interlayers between cathode composite and solid electrolyte. One such method integrated carbon nanotubes or graphite, either alone[161, 205] or in combination with graphene oxide,[206] into the polymer electrolyte. These mixed ion/electron conducting interlayers served to absorb polysulfides, preventing their migration across the polymer electrolyte. In another study, alumina was applied as a thin nanolayer on the cathode to block polysulfides.[207] The introduction of these interlayers between the cathode and polymer electrolyte layers successfully prohibited polysulfide shuttling, leading to an improved cycle life.

4.4 Li anode

Addressing the significant challenge of poor interface stability between the metallic lithium anode and solid electrolytes remains a key focus for achieving prolonged cyclability.[208] A range of engineering strategies have been developed to establish stable interfaces, including the insertion of protective layers at interfaces, implementing chemical and structural modifications to the lithium metal itself, and fine-tuning of solid electrolyte characteristics (Table 3).[20]

Protective interlayers were strategically inserted to suppress parasitic reactions at lithium metal and sulfide electrolyte interfaces, facilitating uniform lithium plating and stripping. A notable example was the application of a silver and carbon mixture (Ag-C) film, which proved effective in anode-free all-solid-state Li metal batteries.[70, 162] In addition, from a processing perspective, this Ag-C layer could be

Table 3 A summary of the electrochemical performance data from the latest research papers on all-solid-state Li metal batteries.

Li Metal anode design	Solid electrolyte	Current density (mA cm^{-2})	Areal capacity (mAh cm^{-2})	Time (h)	Temp. (ºC)	Ref.
SE layer|AgC|Li-20wt% B alloy (AgC=10 μm thick Ag:C in 50:50 wt%)	$Li_{9.54}Si_{1.74}P_{1.44}S_{11.7}Cl_{0.3}$	0.5	2	1800	60	162
SE layer|LNI-CNT|Li (LNI-CNT=15mg Li_7N_2I:CNT in 95:5 wt%)	Li_7N_2I	4	4	600	60	210
SE layer|$Mg_{16}Bi_{84}$|Li	Li_6PS_5Cl	1.2	1.2	2700	25	212
SE layer|CPE|Li (CPE=20 μm thick PEO/LITFSI/Zeolite)	$Li_{1.5}Al_{0.5}Ge_{1.5}(PO_4)_3$	0.1	0.1	1000	60	205
SE layer|LiI|Li (LiI=1.5 μm thick)	$Li_{10}GeP_2S_{12}$	0.15	0.15	800	25	163
SE layer|Li_2NH-Mg|Li-1wt%La alloy	Li_6PS_5Cl	7	7	300	60	214
SE layer|LiF-Li_xMg|Li (LiF-Li_xMg= Mg(TFSI)$_2$/LiTFSI/DME@SE)	$Li_{10}GeP_2S_{12}$	0.2	0.2	140	25	216
PEO/LiFSI/LiN_3|Li	PEO/LiFSI/LiN_3	0.1	0.2	700	70	217
PEO/LiFSI/ $LiC(CN)_3$|Li	PEO/LiTFSI/$LiC(CN)_3$	0.1	0.2	500	70	218
PEO/PGA/Al_2O_3/LiTFSI/Py_{13}TFSI|Li	PEO/PGA/Al_2O_3/LiTFSI/Py_{13}TFSI	0.2	0.2	2800	50	164

easily inserted at interfaces due to its weak adhesion to the substrate, allowing for easy separation and utilization as an interlayer. In addition to silver-carbon mixture, researchers have explored various materials to mix with carbon for use as protective interlayers between the solid electrolyte and Li metal. Wang et al. demonstrated the effectiveness of a mixture of Li_7N-2I and carbon nanotubes, which were inserted as a porous lithiophobic mixed ionic/electronic conductive interlayer.[210] Meanwhile, Ye et al. developed a silicone/graphite composite interlayer that facilitates the mechanical constriction of silicon to facilitate the plating and stripping of Li metal. [211] Another approach involves incorporating a highly ion- and electron-conductive metallics such as magnesium and bismuth, which can form an alloy with lithium.[212] This interlayer helps to mitigate pressure changes during lithium deposition and suppresses the growth of lithium dendrites. In oxide-based all-solid-state Li metal batteries, a polymer composite interlayer comprising PEO, LiTFSI, and zeolite was introduced between $Li_{1.5}Al_{0.5}Ge_{1.5}(PO_4)$ (LAGP) and lithium metal. The purpose of the interlayer addition was to reduce interfacial resistance, contributing to the enhanced electrochemical stability of lithium metal.[205] The construction of an artificial solid electrolyte interlayer (SEI) stands out as a widely adopted strategy for ensuring robust interface stability. The principal function of an artificial SEI is also to impede direct contact between highly reactive lithium and the solid electrolyte while maintaining efficient Li-ion transport. Typically, artificial SEIs are designed with high ionic conductivities and low electronic conductivities. Importantly, they are intended to have robust mechanical properties, capable of withstanding mechanical stresses such as volume changes in lithium or dendrite penetration during cycling. Intelligent artificial SEIs compensate for the inherent drawbacks of some native SEIs, which may lead to continuous and fatal degradation of lithium metal. Various fabrication methods and materials have been employed to build these artificial SEIs on the lithium metal surface. Specifically, a well-known Li-ion conducting binary compound, LiI, was formed through chemical vapor deposition of iodine vapor on the lithium metal surface (Fig. 14A).[163, 213] Other methods to create artificial SEI involved modification of the lithium surface by rolling or rubbing material onto it. Wan et al. introduced Li_2NH-Mg composite interlayer between Li-1wt% La metal and LPSCl.[214] Subsequent heat treatment led to its decomposition, resulting in the formation of Li_6PS_5Cl|LiMgS_x|LiH-Li_3N|LiMgLa multilayers *in situ*. These artificially formed SEIs Li served as a self-passivating layer, effectively suppressing Li dendrites and stabilizing the lithium/electrolyte interface (Fig. 14B). Concurrently, efforts were made to regulate the microstructure of the lithium metal anode, aiming to control the generation of interfacial pores during the stripping process (Fig. 14C).[215]

Moreover, researchers have explored the incorporation of doping or salt additives into solid electrolytes as a strategy to improve the interfaces between lithium metal and solid electrolytes. In sulfide-based all-solid-state batteries, a liquid electrolyte solution comprising Mg(TFSI)$_2$/LiTFSI/DME was carefully applied to the LGPS surface.[216] This process aimed to create a lithiophilic Li_xMg-lithiophobic LiF gradient interphase. Similarly, in polymer-based all-solid-state batteries, various nitrogen-containing additives, including LiN_3,[217] $LiC(CN)_3$,[218] and polyethylene glycol azobenzamide (PGA),[164] were introduced into PEO. This strategic integration constructed SEI enriched with a well-known and favourable component, Li_3N, thereby enhancing the interfacial compatibility of metallic lithium and solid electrolytes (Fig. 14D).

4.5 Binder

Polymeric binders play a crucial role in composite electrodes, facilitating intimate particle contacts to maintain structural robustness and electrode firmness, while also controlling slurry properties.[217] Despite their critical role, research on binders has been relatively underexplored in Li-S batteries. The extensive use of carbon as a conductive agent poses a challenge in binder selection owing to its high surface area, which absorbs a significant amount of solvents, making it difficult to form a homogeneous slurry with modest viscosity. To address this, Yuan et al. studied silicone rubber as a

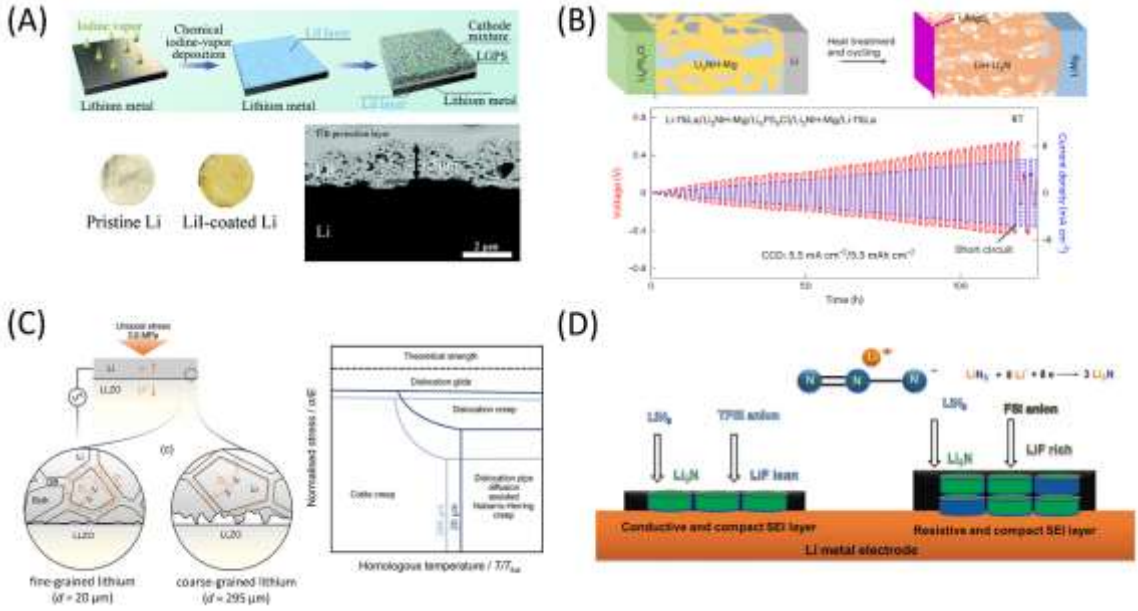

Fig. 14 (A) Schematic illustration of the fabrication of the LiI-coated Li metal *via* chemical vapor deposition, along with top and cross-section images. Reproduced from ref. 163 with permission from Royal Society of Chemistry, Copyright 2022. (B) Schematic illustration of the preparation of the $Li_6PS_5Cl|LiMgS_x|LiH\text{-}Li_3N|LiMg$ interface and voltage profile of the Li metal symmetric cell with developed interlayer tested at increasing current densities. Reproduced from ref. 214 with permission from Nature Publishing Group, copyright 2023. (C) Schematic illustration of creep deformation at the interface for LLZO with fine and coarse grains, accompanied by a creep deformation mechanism map of lithium. Reproduced from ref. 215 with permission from Wiley-VCH Verlag GmbH & Co. KGaA, copyright 2022. (D) Schematic illustration of the reaction mechanism for LiN_3 containing polymer electrolytes. Reproduced from ref. 217 with permission from Wiley-VCH Verlag GmbH & Co. KGaA, copyright 2017.

thickener and binder to be added to a slurry using n-hexane solvent to regulate its viscosity and dispersion.[165] Typically, water and N-methylpyrrolidone (NMP) serve as solvents for slurry mixing in liquid-based batteries. However, in the case of all-solid-state batteries using solid electrolytes with poor chemical stability, like sulfides, these solvents can degrade the ionic conductivity of the solid electrolytes. Consequently, only solvents with low polarity are suitable. Therefore, the range of binder options is limited to those with low polarity that can be dissolved in such solvents. Considering that most highly adhesive binders consist of polar functional groups, this restriction in binder selection can be detrimental to the mechanical integrity of cathode composites. In sulfur cathodes, another challenge arises from the nonpolar characteristics of both carbon and sulfur surfaces, making it difficult to find binders with high adhesion strength to the electrodes. Li et al. plasticized PEO binder as an adhesive polar binder, by incorporating it into LGPS powder and hot-pressing to fabricate membranes (Fig. 15A).[220] However, limited studies have been conducted on the wet electrode processing approach due to the chemically unstable nature of sulfide solid electrolytes complicates the search for suitable solvent-binder pairs. Besides, dry electrode fabrication technology. Employing polytetrafluoroethylene (PTFE) as a binder, has garnered interest in academia and industry (Fig. 15B).[166, 221, 222] Dry electrode processing technology offers comparable advantages over wet processing, particularly for sulfide-based all-solid-state batteries, as it eliminates the challenges associated with solvent selection. Additionally, it is advantageous in terms of manufacturing costs and environmental impacts. When a powder mixture containing electrode materials and a PTFE binder is subjected to shear force during processing, the PTFE fibrillates and connects electrode particles, effectively acting as a binder. While most dry electrode binders consist primarily of PTFE, a recent study explored the use of ethylene vinyl acetate (EVA), a thermoplastic elastomer, as an alternative binder.[223] Although some studies on several binders in all-solid-state sulfur cathodes exist, further efforts are needed to improve both production processes and electrochemical performance. Given the significant volume expansion and contraction of sulfur during charge and discharge cycles, the development of novel binders with high elasticity and adhesivity would be particularly effective in elevating the overall performance of all-solid-state Li-S batteries.

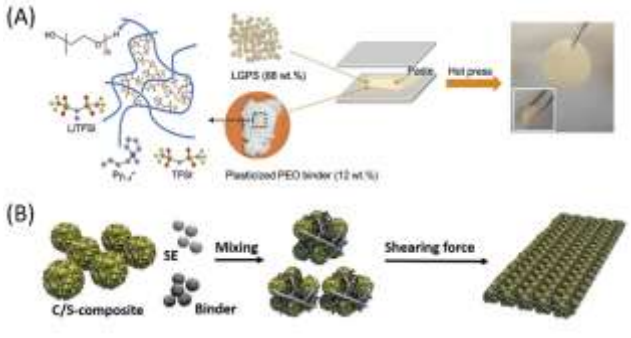

Fig. 15 (A) Schematic illustration of the fabrication process for the LGPS electrolyte layer using plasticized PEO as a binder. Reproduced from ref. 220 with permission from Wiley-VCH Verlag GmbH & Co. KGaA, copyright 2020. (B) Schematic illustration of the fabrication of the sulfur cathode using dry electrode processing. Reproduced from ref. 166 with permission from Wiley-VCH Verlag GmbH & Co. KGaA, copyright 2023.

5. Industrial applications and progress

The manufacture of all-solid-state Li-S cells on an industrial scale faces challenges arising from the high cost of raw materials and the

intricate fabrication processes needed for solid electrolytes, cathode composites, and lithium metal anodes. Addressing these challenges requires the development of more cost-effective and efficient processing methods. Despite the complexities associated with production, the substantial benefits offered by all-solid-state Li-S technology, including its superhigh energy density and enhanced safety features, position it as an appealing choice for large-scale battery applications, particularly in the defense and aerospace sectors. Consequently, the ongoing advancement of this technology holds paramount significance.

5.1 Solid-state electrolytes manufacturing

With the growing interest in all-solid-state batteries across the industry, there is substantial emphasis on advancing solid-state electrolytes manufacturing techniques. While the preparation of polymer and composite electrolytes may be relatively straightforward and well-developed, similar to other commercial polymer engineering processes, the synthesis and manufacturing of ceramic electrolytes require substantial progress.

In the synthesis of sulfide and halide electrolytes, mechanochemical synthesis is commonly employed on a laboratory scale, using ball-milling (Fig. 16A). However, this method is suitable only for small-batch synthesis.[224] At an industrial level, liquid-phase synthesis, encompassing suspension or dissolution-precipitation synthesis, is favoured due to its economic feasibility (Fig. 16B).[225] In suspension synthesis, solid electrolytes are synthesized from precursors dispersed in solvents, while dissolution-precipitation synthesis involves fully dissolving pre-synthesized solid electrolytes in a solvent and then precipitating them. Both liquid-phase syntheses require solvent evaporation and heat treatment to attain the desired crystal structure of the target solid electrolytes. Although the chemical and electrochemical properties, such as ionic conductivity, of sulfides synthesized from current solution methods may not be as robust as those from ball-milling, ongoing research aims to discover more feasible synthesis methods. Hwang et al. employed a novel wet synthesis approach assisted by microwave, resulting in comparatively high Li-ion conductivity with a more facile and time-saving process.[226] In addition, moisture control is another crucial factor in sulfide-based solid electrolyte synthesis. Given the high susceptibility of sulfides to moisture, efforts are required to enhance their air stability and minimize adverse effects during manufacturing. Strategies such as the modification of polyanions, surface coating of sulfide particles,[227] or the addition of H_2S absorbents are proposed to lower reactivity or, at the very least, suppress the toxic influence generated from the hydrolysis of sulfides (Fig. 16C).[228] Although studies have improved the air stability of sulfides, achieving very high Li-ion conductivity simultaneously appears challenging. Instead, carrying out all manufacturing under an inert atmosphere within a glove box or dry room remains an option, albeit one that significantly increases cost burdens and reduces the quantity of material that can be prepared.

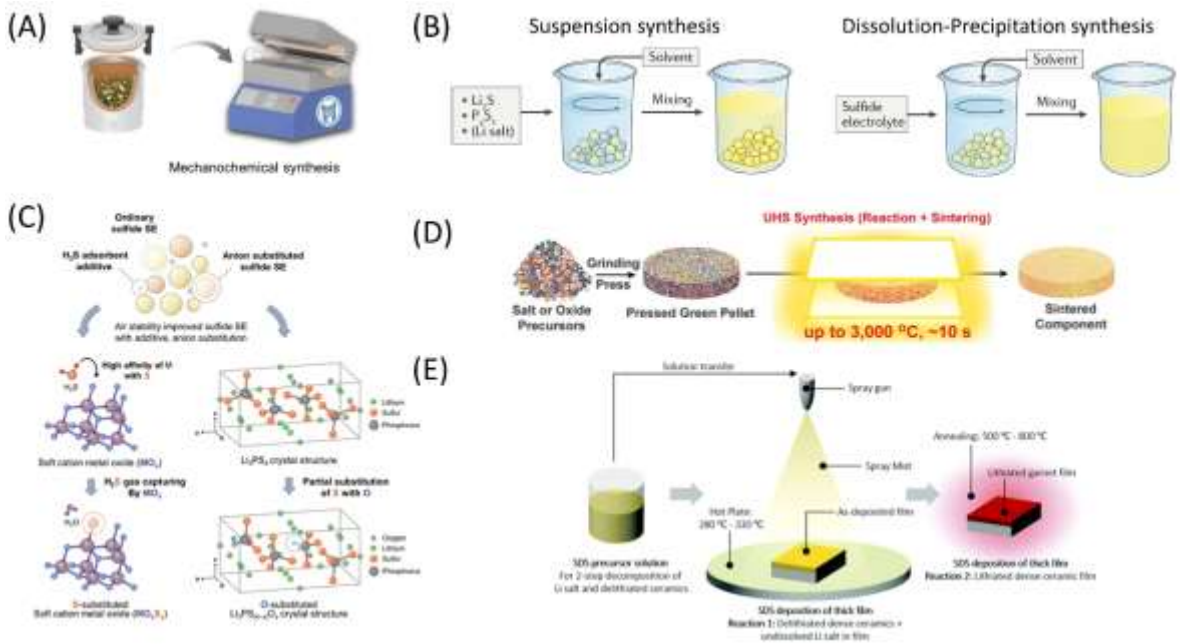

Fig. 16 (A) Schematic illustration of the manufacturing of solid-state electrolytes using mechanochemical synthesis. Reproduced from ref. 224 with permission from Wiley-VCH Verlag GmbH & Co. KGaA, copyright 2022. (B) Schematic illustration of the liquid-phase manufacturing for sulfide electrolytes using suspension or dissolution-precipitation synthesis. Reproduced from ref. 225 with permission from Nature Publishing Group, copyright 2019. (C) Schematic illustration of strategies aimed at alleviating H_2S evolution. Reproduced from ref. 228 with permission from American Chemical Society, copyright 2021. (D) Schematic illustration of the ultrafast high-temperature sintering (UHS) synthesis of oxide electrolytes. Reproduced from ref. 229 with permission from American Association for the Advancement of Science, copyright 2020. (E) Schematic illustration of the sequential decomposition synthesis (SDS) processing of oxide electrolytes. Reproduced from ref. 79 with permission from Royal Society of Chemistry, Copyright 2022.

In the synthesis of oxide electrolytes, a major challenge in the processing line is encountered during the sintering stage. Oxides obtained from solid-state or sol-gel reactions require a sintering process to attain a pure crystalline phase and densify the particles, typically involving high-temperature heating for extended times.[81] To overcome these limitations, innovative approaches, such as ultrafast high-temperature sintering processes[229] and sequential decomposition synthesis methods,[79] were developed (Fig. 16D and 16E). These methods aimed to either reduce the processing time or lower the temperature, ultimately targeting cost reduction.

5.2 Solid-state cell design and manufacturing

Scale-up technologies for solid-state cells are under development, following a trajectory similar to or in comparison with established techniques in conventional liquid-based lithium-ion batteries. Depending on the type of cell architecture for all-solid-state batteries, which can be either a cathode-supported electrolyte and anode two-layer cell or an individual cathode-electrolyte-anode three-layer cell, the manufacturing process involves casting electrode and electrolyte layers, followed by drying and calendaring of these layers, laser cutting, sheet stacking, pressing, and ultimately packaging (Fig. 17). The planar pouch cell format is commonly adopted in solid-state battery manufacturing, offering compatibility with various types of solid electrolytes.[230] For the fabrication of the polymer electrolyte layer, various wet casting techniques, such as drop, blade, spin, and spray coating, are employed. Inorganic solid electrolyte layers are produced through thin-film deposition methods, such as physical vapor deposition (PVD), chemical vapor deposition (CVD), and atomic layer deposition (ALD), mainly for nano-scale layers. Bulk-type solid electrolyte and composite electrode layers are fabricated using methods like tape casting, solution impregnation, hot or cold pressing, extrusion, and 3D printing.[231-235] Tape casting has been extensively utilized to produce thin ceramic layers. In this process, first, the active material powder is blended with conductive additives, a solid electrolyte, and binder into a solvent to make a homogenous slurry. Afterward, the mixture is applied to the current collector foil, which undergoes roll-to-roll processing. Precise thickness control can be achieved by modifying the slurry viscosity and scraper height. Following casting, solvent evaporation and calendaring for densification are carried out.[236] For oxide-based films, additional sintering is necessary. Then, the fabricated electrode and solid electrolyte layers are cut into the desired geometries.[237] Li metal anodes are manufactured through foil extrusion, melt/infiltration, electrochemical deposition, and vapor deposition methods.[5] However, producing very thin lithium foil poses challenges due to its high adhesivity and reactivity. For the assembly of all-solid-state batteries, the cathode, solid electrolyte, and anode layers are sequentially stacked. Additional pressing or heating of the cell stack is then applied to ensure intimate contact between the layers.[238] All-solid-state batteries, which use solid electrolytes exclusively, enable a bipolar architecture where the anode of each cell shares the same bipolar cathode as the neighbouring cell.[239] This design reduces the space needed for welding joints and minimizes packaging requirements. [240] Subsequently, the current collectors are welded and connected to the tabs. Finally, each unit cell is stacked into modules, housed in the case, and sealed.[241, 242]

5.3 Industrial trends and applications

Led by Toyota, which holds one of the largest number of patents related to solid-state batteries, numerous battery and electric vehicle (EV) companies worldwide are actively pursuing the development of bulk solid-state battery technology (Fig. 18). Many automakers are choosing to form joint ventures, such as Toyota with Panasonic, Volkswagen with QuantumScape (based in California, USA), Stellantis and Hyundai with Factorial Energy (based in Massachusetts, USA), or invest in startups. Examples include BMW, Ford, and Hyundai investing in Solid Power (based in Colorado, USA), the Renault-Nissan-Mitsubishi alliance and Hyundai investing in Ionic Materials (based in Massachusetts, USA), and Mercedes investing in ProLogium (based in Taiwan).[243]

A significant focus for many of these companies is the synthesis of solid electrolytes. For instance, Solid Power, QuantumScape, Ganfeng Lithium (based in China), Ohara (based in Japan), Solid Ultrabattery (based in Canada), Murata (based in Japan), NEI (based in New Jersey, USA), and Ampcera are developing sulfide, oxide, or both ceramic electrolytes. Ionic Materials, Brightvolt (based in Washington, USA), Sion Power (based in Arizona, USA), Bollore (based in France), and HydroQuebec (based in Canada) are producing

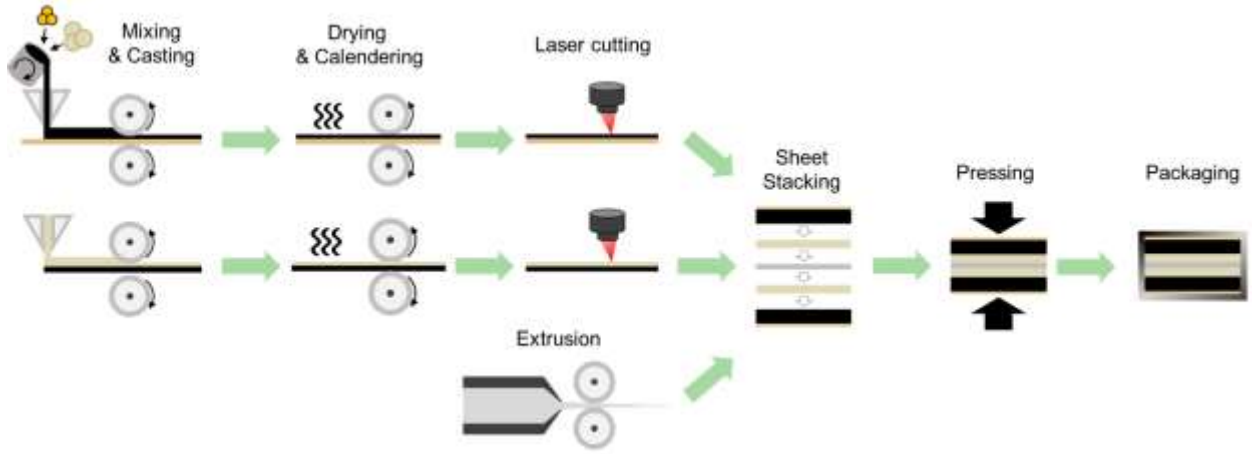

Fig. 17 Schematic illustration of all-solid-state cell manufacturing process adopting individual cathode-electrolyte-anode three-layer cell configuration.

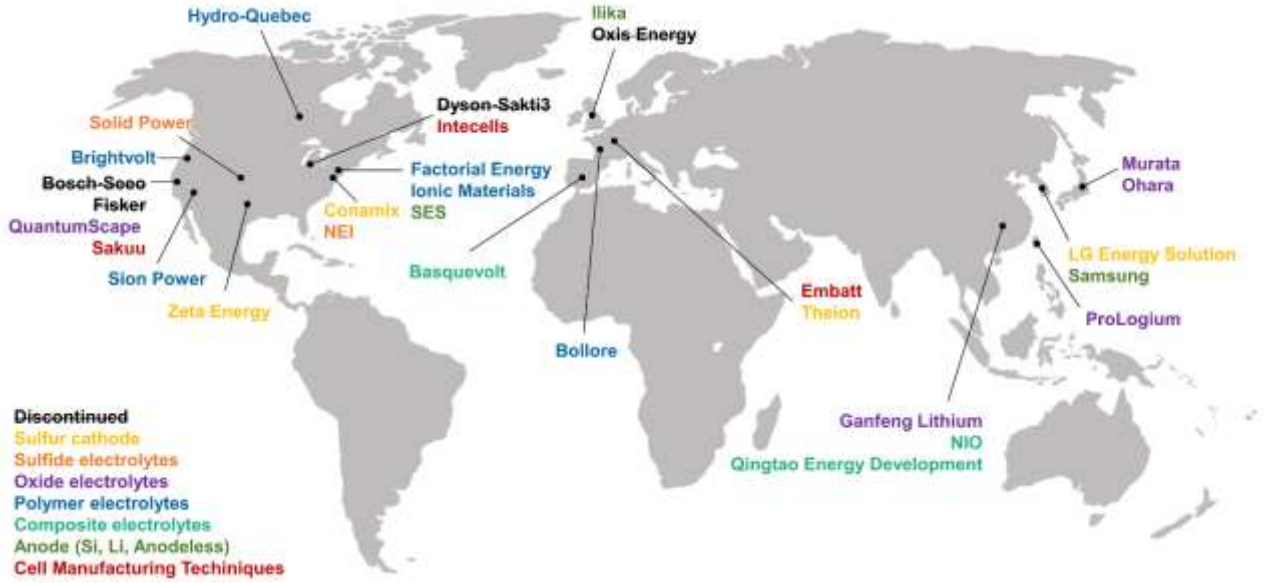

Fig.18 A global overview for all-solid-state battery technologies, encompassing sulfur cathodes, solid electrolytes, anodes, and cell manufacturing.

polymer electrolytes, while Basquevolt (based in Spain), Nio (based in China), and Qingtao Energy Development (based in China) are producing composite electrolytes. In addition to solid electrolytes, various companies including Ilika (based in the UK), SES (based in Massachusetts, USA), and Samsung (based in Korea) are researching anodes such as silicon and lithium metal, as well as anode-less electrodes. Sakuu (based in California, USA), Intecells (based in Michigan, USA), and Embatt (based in Germany) are focusing on cell manufacturing techniques like 3D printing and bipolar electrode fabrication.

Nevertheless, some companies have chosen to discontinue their efforts in solid-state battery development, such as Bosch-Seeo (based in California, USA), Dyson-Sakti3 (based in Michigan, USA), Oxis Energy (based in UK), and Fisker (based in California, USA).

In the case of Li-S batteries, although there is still progress to be made, a few companies like Conamix (based in New York, USA), are commercializing them. Regarding all-solid-state Li-S batteries, there are relatively fewer companies known to be actively working in this area, but Theion (based in Germany) aims to establish itself as a pioneer in this emerging field. Zeta Energy (based in Texas, USA), and LG Energy Solution (based in Korea) are actively developing sulfur cathodes with the aim of commercialization. Regarding all-solid-state Li-S batteries, there are relatively fewer companies known to be actively working in this area, but Theion (based in Germany) aims to establish itself as a pioneer in this emerging field.

The Li-S battery stands out as an exceptionally promising contender for future energy storage devices, thanks to its outstanding gravimetric energy density and economic feasibility. These batteries show great potential for utilization in various large-scale battery applications, including electric automobiles and grid energy systems. Furthermore, the all-solid-state Li-S battery, with its unique advantages of lightweight design and high safety standards, holds tremendous potential for applications in the aerospace industry, particularly in aircraft and advanced air mobility.[244-250]

6. Conclusions and perspectives

In the last decade, substantial progress has been made in advancing the development of all-solid-state Li-S batteries (ASSLSBs), positioning them as a promising choice for the next generation of energy storage technology. ASSLSBs utilize earth-abundant sulfur cathodes and high-capacity lithium metal anodes, with the expectation of achieving remarkably high energy densities. Moreover, the incorporation of non-flammable solid electrolytes adds an extra layer of safety to these innovative solutions. Due to the cost-effectiveness of sulfur compared to metal oxides containing Ni and Co, ASSLSBs present a more economical choice than other ASSBs. The light weight and high capacity of sulfur make ASSBs particularly attractive in terms of gravimetric energy density, which further enables their development in air mobility energy storage applications. However, in terms of volumetric energy density, ASSLSBs do not enjoy a more favourable position. Additionally, the low operating voltage of sulfur may limit the power density of ASSLSBs. Nevertheless, its strongest point lies in its remarkably high energy density. Furthermore, its low operation voltage may provide enhanced safety. While ASSLSBs may not be suitable for all energy storage needs, finding the right application that leverages their advantages—low cost, light weight, high energy density, and safety—is crucial for their successful utilization. The expanding battery market aims for broader applications, including the electrification of vehicles, marine shipping, and aviation. According to the United States Advanced Battery Consortium (USABC) and the Advanced Research Projects Agency-Energy (ARPA-E), cell-level batteries should achieve energy densities and costs of over 700 Wh kg^{-1} and \$ 100 kWh^{-1} for electric vehicles (EVs), and 1000 Wh kg^{-1} and \$ 0.3 kWh^{-1} for energy storage systems (ESS) and aviation (Fig. 19).[251, 252] Given the industry's ambitious goals, achieving these benchmarks is a challenging task, making ASSLSBs stand out. To reach these objectives, achieving a 500 Wh kg^{-1} energy density is the first goal in the near future. This necessitates an areal energy density exceeding 6 mAh cm^{-2}, requiring

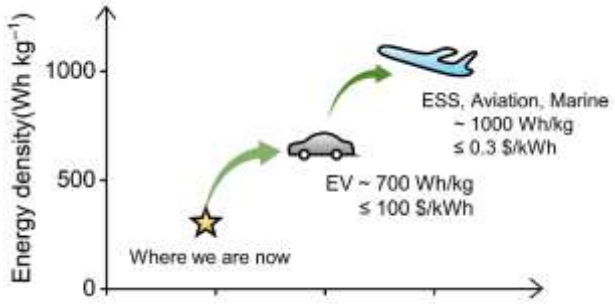

Fig.19 Cell-level battery roadmap required for targeted energy storage applications.

a sulfur loading within the cathode exceeding 4 mg cm^{-2} with a sulfur utilization of 90%. Additionally, a solid electrolyte layer thickness of less than 30 μm and an N/P ratio less than 1.1 are necessary.

The state-of-the-art ASSLSBs primarily rely on sulfide-solid electrolytes. Sulfide electrolytes offer exceptionally high room-temperature ionic conductivity and exhibit good compatibility with sulfur or lithium sulfide active materials. Recent research has made significant progress in improving the energy density of ASSLSBs through innovative material design and processing techniques. Some studies have reported impressive initial areal capacities of over 5-6 mAh cm^{-2}, coupled with a high sulfur loading of 4-5 mg cm^{-2}, while maintaining 90% capacity retention over 100 cycles. However, despite these advancements, several challenges hinder their practical application. Only a few studies have demonstrated long-term and stable electrochemical performance over several hundred cycles. Many research efforts have shown inadequate cell performance during extended cycles. While some have achieved decent capacity retention, they often do so at the expense of sulfur loading, which is reduced to relatively low values. This trade-off results in high retention over longer cycles but overall low areal capacity. Additionally, many reports have conducted cycling tests at elevated temperatures of 60°C to promote Li-ion transport at both the cathode and anode. Furthermore, challenges related to increasing current density (or C-rate) remain critical in most studies. Moreover, the use of Li-In alloy instead of pure Li, which is detrimental to increasing energy density, is a topic left for further research. Beyond sulfide solid electrolytes, there has been limited exploration of alternative materials, and notable breakthroughs in this direction are yet to be achieved.

This review systematically addresses these challenges and provides a comprehensive overview of cutting-edge advancements from laboratory experiences aimed at surmounting these hurdles. Key challenges included insufficient sulfur redox reactions, the severe polysulfide shuttle effect, continuous side reactions in solid electrolytes, lithium metal dendrite propagation, and complexities in scalable manufacturing. To address these challenges, significant efforts have been focused on enhancing the efficiency and reversibility of sulfur utilization, as well as lithium stripping and plating under feasible operating conditions—such as high cell areal capacity and low stack pressure. Innovative cathode designs have been proposed, involving structural and chemical modifications to carbon, the addition of redox mediators within the triphase interface of sulfur-carbon-solid electrolytes, and improvements in cathode fabrication strategies. In-depth insights into the underlying reaction mechanisms in all-solid-state systems have been acquired through the invention of various *in situ*/*operando* characterization techniques. In the future, understanding the working principles of solid-state pouch cells under realistic conditions will become essential to accelerate the commercialization process. Furthermore, a variety of novel solid electrolytes, spanning sulfide, halide, oxide, polymer, and their composites, have been discovered with attributes including superior ionic conductivity, low electronic conductivity, broadened electrochemical stability, robust mechanical properties, and air stability. It is important to note that none of these has emerged as a perfect candidate for ASSLSBs yet, and many efforts to discover new solid electrolytes or combine different solid electrolytes together are continuously under development. Addressing the critical interface between solid electrolytes and lithium metal, various strategies have also been explored, including the addition of protective interlayers and the formation of artificial SEIs. While the optimal manufacturing scheme for all-solid-state batteries remains undetermined, ongoing research is actively addressing this aspect in tandem with optimizing electrode materials.

This review also highlighted industrial research and development, providing valuable insights into the advancement of solid electrolytes and solid-state cells for the practical application of ASSLSBs. With the expanding investment trend in ASSBs, the maturation of relevant technology is eagerly anticipated in the coming years, enhancing its competitiveness and establishing it as a complementary technology to the well-established LIB technology. Consequently, the application scope of ASSLSBs is poised to expand from automotive to electric aircraft, marking a significant step forward toward practical applications.

Conflicts of interest

There are no conflicts to declare.

Acknowledgements

This work was financially supported by the U.S. Department of Energy (DOE), Office of Energy Efficiency and Renewable Energy, Vehicle Technologies Office. Argonne National Laboratory is operated for the DOE Office of Science by UChicago Argonne, LLC, under contract number DE-AC02-06CH11357.

Notes and references

1. N. Yao, L. Heredy and R. Saunders, *J. Electrochem. Soc.*, 1970, **117**, C247.
2. D. R. Vissers and B. S. Tani, US Pat. Pat., 3, 933, 521, 1976.
3. P. G. Bruce, S. A. Freunberger, L. J. Hardwick and J.-M. Tarascon, *Nat. Mater.*, 2012, **11**, 19-29.
4. Z. W. Seh, Y. Sun, Q. Zhang and Y. Cui, *Chem. Soc. Rev.*, 2016, **45**, 5605-5634.
5. F. Duffner, N. Kronemeyer, J. Tübke, J. Leker, M. Winter and R. Schmuch, *Nat. Energy*, 2021, **6**, 123-134.
6. G. Zhou, H. Chen and Y. Cui, *Nat. Energy*, 2022, **7**, 312-319.
7. Z. P. Cano, D. Banham, S. Ye, A. Hintennach, J. Lu, M. Fowler and Z. Chen, *Nat. Energy*, 2018, **3**, 279-289.

8. X. Ji, K. T. Lee and L. F. Nazar, *Nat. Mater.*, 2009, **8**, 500-506.
9. H. Shin, M. Baek, A. Gupta, K. Char, A. Manthiram and J. W. Choi, *Adv. Energy Mater.*, 2020, **10**, 2001456.
10. L.-P. Hou, X.-Q. Zhang, B.-Q. Li and Q. Zhang, *Mater. Today*, 2021, **45**, 62-76.
11. Z. Wei Seh, W. Li, J. J. Cha, G. Zheng, Y. Yang, M. T. McDowell, P.-C. Hsu and Y. Cui, *Nat. Commun.*, 2013, **4**, 1331.
12. Y. Luo, L. Guo, M. Xiao, S. Wang, S. Ren, D. Han and Y. Meng, *J. Mater. Chem. A*, 2020, **8**, 4629-4646.
13. L. Huang, J. Li, B. Liu, Y. Li, S. Shen, S. Deng, C. Lu, W. Zhang, Y. Xia, G. Pan, X. Wang, Q. Xiong, X. Xia and J. Tu, *Adv. Funct. Mater.*, 2020, **30**, 1910375.
14. Y. Chen, T. Wang, H. Tian, D. Su, Q. Zhang and G. Wang, *Adv. Mater.*, 2021, **33**, 2003666.
15. X. Yang, J. Luo and X. Sun, *Chem. Soc. Rev.*, 2020, **49**, 2140-2195.
16. Y. Chen, Z. Wang, X. Li, X. Yao, C. Wang, Y. Li, W. Xue, D. Yu, S. Y. Kim, F. Yang, A. Kushima, G. Zhang, H. Huang, N. Wu, Y.-W. Mai, J. B. Goodenough and J. Li, *Nature*, 2020, **578**, 251-255.
17. C. Xing, H. Chen, S. Qian, Z. Wu, A. Nizami, X. Li, S. Zhang and C. Lai, *Chem*, 2022, **8**, 1201-1230.
18. Y. Cui, J. Wan, Y. Ye, K. Liu, L.-Y. Chou and Y. Cui, *Nano Lett.*, 2020, **20**, 1686-1692.
19. S. Wang, Y. Wu, T. Ma, L. Chen, H. Li and F. Wu, *ACS Nano*, 2022, **16**, 16158-16176.
20. Green Car Congress, DOE Awarding $209M to 26 National Lab Projects; EVs, Batteries and Connected Vehicles, https://www.greencarcongress.com/2021/10/20211028-doe.html, (accessed December 2, 2023).
21. Green Car Congress, Fraunhofer Leading "MaSSiF" Research Project on Solid-State Sulfur-Silicon Batteries, https://www.greencarcongress.com/2023/04/20230426-massif.html, (accessed December 2, 2023).
22. NASA, NASA Seeks to Create a Better Battery with SABERS, https://www.nasa.gov/feature/nasa-seeks-to-create-a-better-battery-with-sabers, (accessed December 2, 2023).
23. Green Car Congress, Battery Start-Up Theion Unveils Li-S "Crystal Battery" for Mobile Applications, https://www.greencarcongress.com/2022/03/20220330-theion.html, (accessed December 2, 2023).
24. A. Manthiram, X. Yu and S. Wang, *Nat. Rev. Mater.*, 2017, **2**, 16103.
25. J. C. Barbosa, R. Gonçalves, C. M. Costa and S. Lanceros-Méndez, *ACS Omega*, 2022, **7**, 14457-14464.
26. Q. Zhao, S. Stalin, C.-Z. Zhao and L. A. Archer, *Nat. Rev. Mater.*, 2020, **5**, 229-252.
27. H. Wang, L. Sheng, G. Yasin, L. Wang, H. Xu and X. He, *Energy Storage Mater.*, 2020, **33**, 188-215.
28. Y. An, X. Han, Y. Liu, A. Azhar, J. Na, A. K. Nanjundan, S. Wang, J. Yu and Y. Yamauchi, *Small*, 2022, **18**, 2103617.
29. P.-F. Wang, X. He, Z.-C. Lv, H. Song, X. Song, T.-F. Yi, N. Xu, P. He and H. Zhou, *Adv. Funct. Mater.*, 2023, **33**, 2211074.
30. G. G. Eshetu, X. Judez, C. Li, M. Martinez-Ibañez, I. Gracia, O. Bondarchuk, J. Carrasco, L. M. Rodriguez-Martinez, H. Zhang and M. Armand, *J. Am. Chem. Soc.*, 2018, **140**, 9921-9933.
31. S. Liu, W. Liu, D. Ba, Y. Zhao, Y. Ye, Y. Li and J. Liu, *Adv. Mater.*, 2023, **35**, 2110423.
32. X. Judez, H. Zhang, C. Li, J. A. González-Marcos, Z. Zhou, M. Armand and L. M. Rodriguez-Martinez, *J. Phys. Chem. Lett.*, 2017, **8**, 1956-1960.
33. R. Fang, H. Xu, B. Xu, X. Li, Y. Li and J. B. Goodenough, *Adv. Funct. Mater.*, 2021, **31**, 2001812.
34. Y. Ji, K. Yang, M. Liu, S. Chen, X. Liu, B. Yang, Z. Wang, W. Huang, Z. Song, S. Xue, Y. Fu, L. Yang, T. S. Miller and F. Pan, *Adv. Funct. Mater.*, 2021, **31**, 2104830.
35. Y. Yang, H. Chen, J. Wan, R. Xu, P. Zhang, W. Zhang, S. T. Oyakhire, S. C. Kim, D. T. Boyle, Y. Peng, Y. Ma and Y. Cui, *Adv. Energy Mater.*, 2022, **12**, 2201160.
36. Z. Ao, Y. Zou, H. Zou, Y. Huang and N. Chen, *Chem.Eur. J.*, 2022, **28**, e202200543.
37. L. Zhong, S. Wang, M. Xiao, W. Liu, D. Han, Z. Li, J. Qin, Y. Li, S. Zhang, S. Huang and Y. Meng, *Energy Storage Mater.*, 2021, **41**, 563-570.
38. J. Sheng, Q. Zhang, C. Sun, J. Wang, X. Zhong, B. Chen, C. Li, R. Gao, Z. Han and G. Zhou, *Adv. Funct. Mater.*, 2022, **32**, 2203272.
39. C. Yang, Q. Wu, W. Xie, X. Zhang, A. Brozena, J. Zheng, M. N. Garaga, B. H. Ko, Y. Mao, S. He, Y. Gao, P. Wang, M. Tyagi, F. Jiao, R. Briber, P. Albertus, C. Wang, S. Greenbaum, Y.-Y. Hu, A. Isogai, M. Winter, K. Xu, Y. Qi and L. Hu, *Nature*, 2021, **598**, 590-596.
40. P. Prakash, B. Fall, J. Aguirre, L. A. Sonnenberg, P. R. Chinnam, S. Chereddy, D. A. Dikin, A. Venkatnathan, S. L. Wunder and M. J. Zdilla, *Nat. Mater.*, 2023, **22**, 627-635.
41. Y. Zheng, Y. Yao, J. Ou, M. Li, D. Luo, H. Dou, Z. Li, K. Amine, A. Yu and Z. Chen, *Chem. Soc. Rev.*, 2020, **49**, 8790-8839.
42. S. Tang, W. Guo and Y. Fu, *Adv. Energy Mater.*, 2021, **11**, 2000802.
43. X. Li, D. Wang, H. Wang, H. Yan, Z. Gong and Y. Yang, *ACS Appl. Mater. Interfaces*, 2019, **11**, 22745-22753.
44. Y. Zhang, R. Chen, S. Wang, T. Liu, B. Xu, X. Zhang, X. Wang, Y. Shen, Y.-H. Lin, M. Li, L.-Z. Fan, L. Li and C.-W. Nan, *Energy Storage Mater.*, 2020, **25**, 145-153.
45. Y. Su, X. Zhang, C. Du, Y. Luo, J. Chen, J. Yan, D. Zhu, L. Geng, S. Liu, J. Zhao, Y. Li, Z. Rong, Q. Huang, L. Zhang, Y. Tang and J. Huang, *Small*, 2022, **18**, 2202069.
46. X. Tao, Y. Liu, W. Liu, G. Zhou, J. Zhao, D. Lin, C. Zu, O. Sheng, W. Zhang, H.-W. Lee and Y. Cui, *Nano Lett.*, 2017, **17**, 2967-2972.
47. E. Temeche, X. Zhang and R. M. Laine, *ACS Appl. Mater. Interfaces*, 2020, **12**, 30353-30364.
48. S. Bag, C. Zhou, P. J. Kim, V. G. Pol and V. Thangadurai, *Energy Storage Mater.*, 2020, **24**, 198-207.
49. P. Shi, J. Ma, M. Liu, S. Guo, Y. Huang, S. Wang, L. Zhang, L. Chen, K. Yang, X. Liu, Y. Li, X. An, D. Zhang, X. Cheng, Q. Li, W. Lv, G. Zhong, Y.-B. He and F. Kang, *Nat. Nanotech.*, 2023, DOI: 10.1038/s41565-023-01341-2.
50. X. Zhang, T. Zhang, Y. Shao, H. Cao, Z. Liu, S. Wang and X. Zhang, *ACS Sustain. Chem. Eng.*, 2021, **9**, 5396-5404.
51. X. Judez, H. Zhang, C. Li, G. G. Eshetu, Y. Zhang, J. A. González-Marcos, M. Armand and L. M. Rodriguez-Martinez, *J. Phys. Chem. Lett.*, 2017, **8**, 3473-3477.

52. B. Wei, S. Huang, Y. Song, X. Wang, M. Liu, H. Jin and G. Cao, *J. Mater. Chem. A*, 2023, **11**, 11426-11435.
53. X. Yin, L. Wang, Y. Kim, N. Ding, J. Kong, D. Safanama, Y. Zheng, J. Xu, D. V. M. Repaka, K. Hippalgaonkar, S. W. Lee, S. Adams and G. W. Zheng, *Adv. Sci.*, 2020, **7**, 2001303.
54. P. Zhai, N. Peng, Z. Sun, W. Wu, W. Kou, G. Cui, K. Zhao and J. Wang, *J. Mater. Chem. A*, 2020, **8**, 23344-23353.
55. S. Suriyakumar, S. Gopi, M. Kathiresan, S. Bose, E. B. Gowd, J. R. Nair, N. Angulakshmi, G. Meligrana, F. Bella, C. Gerbaldi and A. M. Stephan, *Electrochim. Acta.*, 2018, **285**, 355-364.
56. J. Zheng and Y.-Y. Hu, *ACS Appl. Mater. Interfaces*, 2018, **10**, 4113-4120.
57. J. Fu, Z. Li, X. Zhou and X. Guo, *Mater. Adv.*, 2022, **3**, 3809-3819.
58. C. Hu, Y. Shen, M. Shen, X. Liu, H. Chen, C. Liu, T. Kang, F. Jin, L. Li, J. Li, Y. Li, N. Zhao, X. Guo, W. Lu, B. Hu and L. Chen, *J. Am. Chem. Soc.*, 2020, **142**, 18035-18041.
59. J. Wu, S. Liu, F. Han, X. Yao and C. Wang, *Adv. Mater.*, 2021, **33**, 2000751.
60. Y. Duan, X. Bai, T. Yu, Y. Rong, Y. Wu, X. Wang, J. Yang and J. Wang, *J. Energy Storage*, 2022, **55**, 105382.
61. P. Bonnick, K. Niitani, M. Nose, K. Suto, T. S. Arthur and J. Muldoon, *J. Mater. Chem. A*, 2019, **7**, 24173-24179.
62. H.-J. Deiseroth, S.-T. Kong, H. Eckert, J. Vannahme, C. Reiner, T. Zaiß and M. Schlosser, *Angew. Chem. Int. Ed.*, 2008, **47**, 755-758.
63. S. V. Patel, S. Banerjee, H. Liu, P. Wang, P.-H. Chien, X. Feng, J. Liu, S. P. Ong and Y.-Y. Hu, *Chem. Mater.*, 2021, **33**, 1435-1443.
64. N. Kamaya, K. Homma, Y. Yamakawa, M. Hirayama, R. Kanno, M. Yonemura, T. Kamiyama, Y. Kato, S. Hama, K. Kawamoto and A. Mitsui, *Nat. Mater.*, 2011, **10**, 682-686.
65. K. J. Kim, M. Balaish, M. Wadaguchi, L. Kong and J. L. M. Rupp, *Adv. Energy Mater.*, 2021, **11**, 2002689.
66. L. Zhou, N. Minafra, W. G. Zeier and L. F. Nazar, *Acc. Chem. Res.*, 2021, **54**, 2717-2728.
67. Y. Kato, S. Hori, T. Saito, K. Suzuki, M. Hirayama, A. Mitsui, M. Yonemura, H. Iba and R. Kanno, *Nat. Energy*, 2016, **1**, 16030.
68. Y. Nikodimos, C.-J. Huang, B. W. Taklu, W.-N. Su and B. J. Hwang, *Energy Environ. Sci.*, 2022, **15**, 991-1033.
69. T. K. Schwietert, V. A. Arszelewska, C. Wang, C. Yu, A. Vasileiadis, N. J. J. de Klerk, J. Hageman, T. Hupfer, I. Kerkamm, Y. Xu, E. van der Maas, E. M. Kelder, S. Ganapathy and M. Wagemaker, *Nat. Mater.*, 2020, **19**, 428-435.
70. Y.-G. Lee, S. Fujiki, C. Jung, N. Suzuki, N. Yashiro, R. Omoda, D.-S. Ko, T. Shiratsuchi, T. Sugimoto, S. Ryu, J. H. Ku, T. Watanabe, Y. Park, Y. Aihara, D. Im and I. T. Han, *Nat. Energy*, 2020, **5**, 299-308.
71. J. Lee and J. W. Choi, *EcoMat*, 2022, **4**, e12193.
72. Y. Xiao, Y. Wang, S.-H. Bo, J. C. Kim, L. J. Miara and G. Ceder, *Nat. Rev. Mater.*, 2020, **5**, 105-126.
73. M. A. Subramanian, R. Subramanian and A. Clearfield, *Solid State Ion.*, 1986, **18-19**, 562-569.
74. H. Y. P. Hong, *Mater. Res. Bull.*, 1978, **13**, 117-124.
75. R. Murugan, V. Thangadurai and W. Weppner, *Angew. Chem. Int. Ed.*, 2007, **46**, 7778-7781.
76. Y. Inaguma, C. Liquan, M. Itoh, T. Nakamura, T. Uchida, H. Ikuta and M. Wakihara, *Solid State Commun.*, 1993, **86**, 689-693.
77. Y. Zhao and L. L. Daemen, *J. Am. Chem. Soc.*, 2012, **134**, 15042-15047.
78. X. Huang, C. Liu, Y. Lu, T. Xiu, J. Jin, M. E. Badding and Z. Wen, *J. Power Sources*, 2018, **382**, 190-197.
79. Z. D. Hood, Y. Zhu, L. J. Miara, W. S. Chang, P. Simons and J. L. M. Rupp, *Energy Environ. Sci.*, 2022, **15**, 2927-2936.
80. S. Gu, X. Huang, Q. Wang, J. Jin, Q. Wang, Z. Wen and R. Qian, *J. Mater. Chem. A*, 2017, **5**, 13971-13975.
81. R. Wei, S. Chen, T. Gao and W. Liu, *Nano Select*, 2021, **2**, 2256-2274.
82. W. D. Richards, L. J. Miara, Y. Wang, J. C. Kim and G. Ceder, *Chem. Mater.*, 2016, **28**, 266-273.
83. Y.-N. Yang, Y.-X. Li, Y.-Q. Li and T. Zhang, *Nat. Commun.*, 2020, **11**, 5519.
84. W. Feng, L. Zhu, X. Dong, Y. Wang, Y. Xia and F. Wang, *Adv. Mater.*, 2023, **35**, 2210365.
85. X. Li, J. Liang, X. Yang, K. R. Adair, C. Wang, F. Zhao and X. Sun, *Energy Environ. Sci.*, 2020, **13**, 1429-1461.
86. T. Asano, A. Sakai, S. Ouchi, M. Sakaida, A. Miyazaki and S. Hasegawa, *Adv. Mater.*, 2018, **30**, 1803075.
87. R. Schlem, S. Muy, N. Prinz, A. Banik, Y. Shao-Horn, M. Zobel and W. G. Zeier, *Adv. Energy Mater.*, 2020, **10**, 1903719.
88. J. Liang, X. Li, S. Wang, K. R. Adair, W. Li, Y. Zhao, C. Wang, Y. Hu, L. Zhang, S. Zhao, S. Lu, H. Huang, R. Li, Y. Mo and X. Sun, *J. Am. Chem. Soc.*, 2020, **142**, 7012-7022.
89. X. Shi, Z. Zeng, M. Sun, B. Huang, H. Zhang, W. Luo, Y. Huang, Y. Du and C. Yan, *Nano Lett.*, 2021, **21**, 9325-9331.
90. H. Kwak, D. Han, J. Lyoo, J. Park, S. H. Jung, Y. Han, G. Kwon, H. Kim, S.-T. Hong, K.-W. Nam and Y. S. Jung, *Adv. Energy Mater.*, 2021, **11**, 2003190.
91. K.-H. Park, K. Kaup, A. Assoud, Q. Zhang, X. Wu and L. F. Nazar, *ACS Energy Lett.*, 2020, **5**, 533-539.
92. L. M. Riegger, R. Schlem, J. Sann, W. G. Zeier and J. Janek, *Angew. Chem. Int. Ed.*, 2021, **60**, 6718-6723.
93. W. Kim, J. Noh, S. Lee, K. Yoon, S. Han, D. Kil, S. Yu, K.-H. Ko and K. Kang, *Adv. Mater.*, 2023, **35**, 2301631.
94. Y. Nikodimos, W.-N. Su and B. J. Hwang, *Adv. Energy Mater.*, 2023, **13**, 2202854.
95. C. Rosenbach, F. Walther, J. Ruhl, M. Hartmann, T. A. Hendriks, S. Ohno, J. Janek and W. G. Zeier, *Adv. Energy Mater.*, 2023, **13**, 2203673.
96. S. Wang, X. Xu, C. Cui, C. Zeng, J. Liang, J. Fu, R. Zhang, T. Zhai and H. Li, *Adv. Funct. Mater.*, 2022, **32**, 2108805.
97. B. Ding, J. Wang, Z. Fan, S. Chen, Q. Lin, X. Lu, H. Dou, A. Kumar Nanjundan, G. Yushin, X. Zhang and Y. Yamauchi, *Mater. Today*, 2020, **40**, 114-131.
98. S. Ohno and W. G. Zeier, *Acc. Mater. Res.*, 2021, **2**, 869-880.
99. A. Jena, Z. Tong, B. Bazri, K. Iputera, H. Chang, S.-F. Hu and R.-S. Liu, *J. Phys. Chem. C*, 2021, **125**, 16921-16937.
100. L. Zhang, H. Fan, Y. Dang, Q. Zhuang, H. Arandiyan, Y. Wang, N. Cheng, H. Sun, H. H. Pérez Garza, R. Zheng, Z. Wang, S. S. Mofarah, P. Koshy, S. K. Bhargava, Y. Cui, Z. Shao and Y. Liu, *Mater. Horiz.*, 2023, **10**, 1479-1538.

101. K. N. Wood, K. X. Steirer, S. E. Hafner, C. Ban, S. Santhanagopalan, S.-H. Lee and G. Teeter, *Nat. Commun.*, 2018, **9**, 2490.
102. S. H. Kim, K. Kim, H. Choi, D. Im, S. Heo and H. S. Choi, *J. Mater. Chem. A*, 2019, **7**, 13650-13657.
103. F. Strauss, D. Kitsche, Y. Ma, J. H. Teo, D. Goonetilleke, J. Janek, M. Bianchini and T. Brezesinski, *Adv. Energy Sustain. Res.*, 2021, **2**, 2100004.
104. Z. Zhang, Y. Wang, T. Liu, G. Li, J. Ma, J. Zhang, P. Han, S. Dong, X. Yan, Y. Tang and G. Cui, *Nano Res.*, 2023, **16**, 8139-8158.
105. R. Bradbury, G. F. Dewald, M. A. Kraft, T. Arlt, N. Kardjilov, J. Janek, I. Manke, W. G. Zeier and S. Ohno, *Adv. Energy Mater.*, 2023, **13**, 2203426.
106. Z. Wang, Y. Tang, L. Zhang, M. Li, Z. Shan and J. Huang, *Small*, 2020, **16**, 2001899.
107. D. Cao, X. Sun, F. Li, S.-M. Bak, T. Ji, M. Geiwitz, K. S. Burch, Y. Du, G. Yang and H. Zhu, *Angew. Chem. Int. Ed.*, 2023, **62**, e202302363.
108. Y. Xiao, K. Yamamoto, Y. Matsui, T. Watanabe, A. Sakuda, K. Nakanishi, T. Uchiyama, A. Hayashi, S. Shingubara, M. Tatsumisago, M. Ishikawa, M. Watanabe and Y. Uchimoto, *ACS Appl. Energy Mater.*, 2021, **4**, 186-193.
109. M. L. Holekevi Chandrappa, J. Qi, C. Chen, S. Banerjee and S. P. Ong, *J. Am. Chem. Soc.*, 2022, **144**, 18009-18022.
110. Y.-X. Song, Y. Shi, J. Wan, S.-Y. Lang, X.-C. Hu, H.-J. Yan, B. Liu, Y.-G. Guo, R. Wen and L.-J. Wan, *Energy Environ. Sci.*, 2019, **12**, 2496-2506.
111. Y.-X. Song, J. Wan, H.-J. Guo, Y. Shi, X.-C. Hu, B. Liu, H.-J. Yan, R. Wen and L.-J. Wan, *Energy Storage Mater.*, 2021, **41**, 642-649.
112. H. Marceau, C.-S. Kim, A. Paolella, S. Ladouceur, M. Lagacé, M. Chaker, A. Vijh, A. Guerfi, C. M. Julien, A. Mauger, M. Armand, P. Hovington and K. Zaghib, *J. Power Sources*, 2016, **319**, 247-254.
113. S. Ohno, R. Koerver, G. Dewald, C. Rosenbach, P. Titscher, D. Steckermeier, A. Kwade, J. Janek and W. G. Zeier, *Chem. Mater.*, 2019, **31**, 2930-2940.
114. K. Kisu, S. Kim, R. Yoshida, H. Oguchi, N. Toyama and S.-i. Orimo, *J. Energy Chem.*, 2020, **50**, 424-429.
115. C. Zheng, K. Wang, L. Li, H. Huang, C. Liang, Y. Gan, X. He, W. Zhang and J. Zhang, *Front. Energy Res.*, 2021, **8**.
116. J. Lee, K. Heo, Y.-W. Song, D. Hwang, M.-Y. Kim, H. Jeong, D.-C. Shin and J. Lim, *J. Electrochem. Sci. Technol.*, 2022, **13**, 199-207.
117. D. H. S. Tan, E. A. Wu, H. Nguyen, Z. Chen, M. A. T. Marple, J.-M. Doux, X. Wang, H. Yang, A. Banerjee and Y. S. Meng, *ACS Energy Lett.*, 2019, **4**, 2418-2427.
118. L. E. Camacho-Forero and P. B. Balbuena, *Chem. Mater.*, 2020, **32**, 360-373.
119. C. Yu, J. Hageman, S. Ganapathy, L. van Eijck, L. Zhang, K. R. Adair, X. Sun and M. Wagemaker, *J. Mater. Chem. A*, 2019, **7**, 10412-10421.
120. E. Nagai, T. S. Arthur, P. Bonnick, K. Suto and J. Muldoon, *MRS Adv.*, 2019, **4**, 2627-2634.
121. S. Wang, M. Tang, Q. Zhang, B. Li, S. Ohno, F. Walther, R. Pan, X. Xu, C. Xin, W. Zhang, L. Li, Y. Shen, F. H. Richter, J. Janek and C.-W. Nan, *Adv. Energy Mater.*, 2021, **11**, 2101370.
122. H. Gamo, K. Hikima and A. Matsuda, *Chem. Mater.*, 2022, **34**, 10952-10963.
123. S. Ohno, C. Rosenbach, G. F. Dewald, J. Janek and W. G. Zeier, *Adv. Funct. Mater.*, 2021, **31**, 2010620.
124. F. Strauss, J. H. Teo, J. Maibach, A. Y. Kim, A. Mazilkin, J. Janek and T. Brezesinski, *ACS Appl. Mater. Interfaces*, 2020, **12**, 57146-57154.
125. T. Krauskopf, F. H. Richter, W. G. Zeier and J. Janek, *Chem. Rev.*, 2020, **120**, 7745-7794.
126. M. Golozar, A. Paolella, H. Demers, S. Savoie, G. Girard, N. Delaporte, R. Gauvin, A. Guerfi, H. Lorrmann and K. Zaghib, *Sci. Rep.*, 2020, **10**, 18410.
127. E. Kazyak, R. Garcia-Mendez, W. S. LePage, A. Sharafi, A. L. Davis, A. J. Sanchez, K.-H. Chen, C. Haslam, J. Sakamoto and N. P. Dasgupta, *Matter*, 2020, **2**, 1025-1048.
128. S. Luo, Z. Wang, X. Li, X. Liu, H. Wang, W. Ma, L. Zhang, L. Zhu and X. Zhang, *Nat. Commun.*, 2021, **12**, 6968.
129. Z. Liang, Y. Xiang, K. Wang, J. Zhu, Y. Jin, H. Wang, B. Zheng, Z. Chen, M. Tao, X. Liu, Y. Wu, R. Fu, C. Wang, M. Winter and Y. Yang, *Nat. Commun.*, 2023, **14**, 259.
130. K. J. Harry, D. T. Hallinan, D. Y. Parkinson, A. A. MacDowell and N. P. Balsara, *Nat. Mater.*, 2014, **13**, 69-73.
131. N. G. Yadav, N. Folastre, M. Bolmont, A. Jamali, M. Morcrette and C. Davoisne, *J. Mater. Chem. A*, 2022, **10**, 17142-17155.
132. H. Liu, X.-B. Cheng, J.-Q. Huang, H. Yuan, Y. Lu, C. Yan, G.-L. Zhu, R. Xu, C.-Z. Zhao, L.-P. Hou, C. He, S. Kaskel and Q. Zhang, *ACS Energy Lett.*, 2020, **5**, 833-843.
133. Z. Ning, D. S. Jolly, G. Li, R. De Meyere, S. D. Pu, Y. Chen, J. Kasemchainan, J. Ihli, C. Gong, B. Liu, D. L. R. Melvin, A. Bonnin, O. Magdysyuk, P. Adamson, G. O. Hartley, C. W. Monroe, T. J. Marrow and P. G. Bruce, *Nat. Mater.*, 2021, **20**, 1121-1129.
134. M. B. Dixit, N. Singh, J. P. Horwath, P. D. Shevchenko, M. Jones, E. A. Stach, T. S. Arthur and K. B. Hatzell, *Matter*, 2020, **3**, 2138-2159.
135. J. Tippens, J. C. Miers, A. Afshar, J. A. Lewis, F. J. Q. Cortes, H. Qiao, T. S. Marchese, C. V. Di Leo, C. Saldana and M. T. McDowell, *ACS Energy Lett.*, 2019, **4**, 1475-1483.
136. T. Fuchs, C. G. Haslam, A. C. Moy, C. Lerch, T. Krauskopf, J. Sakamoto, F. H. Richter and J. Janek, *Adv. Energy Mater.*, 2022, **12**, 2201125.
137. J. Kasemchainan, S. Zekoll, D. Spencer Jolly, Z. Ning, G. O. Hartley, J. Marrow and P. G. Bruce, *Nat. Mater.*, 2019, **18**, 1105-1111.
138. M. Yang, Y. Liu, A. M. Nolan and Y. Mo, *Adv. Mater.*, 2021, **33**, 2008081.
139. J. A. Lewis, F. J. Q. Cortes, Y. Liu, J. C. Miers, A. Verma, B. S. Vishnugopi, J. Tippens, D. Prakash, T. S. Marchese, S. Y. Han, C. Lee, P. P. Shetty, H.-W. Lee, P. Shevchenko, F. De Carlo, C. Saldana, P. P. Mukherjee and M. T. McDowell, *Nat. Mater.*, 2021, **20**, 503-510.
140. X. Gao, B. Liu, B. Hu, Z. Ning, D. S. Jolly, S. Zhang, J. Perera, J. Bu, J. Liu, C. Doerrer, E. Darnbrough, D. Armstrong, P. S. Grant and P. G. Bruce, *Joule*, 2022, **6**, 636-646.

141. F. Zhang, Y. Guo, L. Zhang, P. Jia, X. Liu, P. Qiu, H. Zhang and J. Huang, *eTransportation*, 2023, **15**, 100220.
142. J.-M. Doux, H. Nguyen, D. H. S. Tan, A. Banerjee, X. Wang, E. A. Wu, C. Jo, H. Yang and Y. S. Meng, *Adv. Energy Mater.*, 2020, **10**, 1903253.
143. M. J. Wang, R. Choudhury and J. Sakamoto, *Joule*, 2019, **3**, 2165-2178.
144. X. Zhang, Q. J. Wang, K. L. Harrison, S. A. Roberts and S. J. Harris, *Cell Rep. Phys. Sci.*, 2020, **1**, 100012.
145. P. Albertus, V. Anandan, C. Ban, N. Balsara, I. Belharouak, J. Buettner-Garrett, Z. Chen, C. Daniel, M. Doeff, N. J. Dudney, B. Dunn, S. J. Harris, S. Herle, E. Herbert, S. Kalnaus, J. A. Libera, D. Lu, S. Martin, B. D. McCloskey, M. T. McDowell, Y. S. Meng, J. Nanda, J. Sakamoto, E. C. Self, S. Tepavcevic, E. Wachsman, C. Wang, A. S. Westover, J. Xiao and T. Yersak, *ACS Energy Lett.*, 2021, **6**, 1399-1404.
146. D. H. S. Tan, Y. S. Meng and J. Jang, *Joule*, 2022, **6**, 1755-1769.
147. S. H. Jung, U.-H. Kim, J.-H. Kim, S. Jun, C. S. Yoon, Y. S. Jung and Y.-K. Sun, *Adv. Energy Mater.*, 2020, **10**, 1903360.
148. C. Lee, S. Y. Han, J. A. Lewis, P. P. Shetty, D. Yeh, Y. Liu, E. Klein, H.-W. Lee and M. T. McDowell, *ACS Energy Lett.*, 2021, **6**, 3261-3269.
149. B. Fan, Z. Guan, L. Wu, S. Zhang, M. Tan, Z. Luo, X. Zhang, H. Ma and B. Xue, *J. Am. Ceram. Soc.*, 2023, **106**, 5781-5794.
150. H. Nagata, Y. Chikusa and J. Akimoto, *J. Power Sources*, 2020, **453**, 227905.
151. H. Duan, L. Li, X. Fu, Y. Deng and G. Chen, *Chem. Eng. J.*, 2022, **450**, 138208.
152. D. Wang, L.-J. Jhang, R. Kou, M. Liao, S. Zheng, H. Jiang, P. Shi, G.-X. Li, K. Meng and D. Wang, *Nat. Commun.*, 2023, **14**, 1895.
153. T. Hakari, Y. Fujita, M. Deguchi, Y. Kawasaki, M. Otoyama, Y. Yoneda, A. Sakuda, M. Tatsumisago and A. Hayashi, *Adv. Funct. Mater.*, 2022, **32**, 2106174.
154. X. Yao, N. Huang, F. Han, Q. Zhang, H. Wan, J. P. Mwizerwa, C. Wang and X. Xu, *Adv. Energy Mater.*, 2017, **7**, 1602923.
155. A. S. Alzahrani, M. Otaki, D. Wang, Y. Gao, T. S. Arthur, S. Liu and D. Wang, *ACS Energy Lett.*, 2021, **6**, 413-418.
156. A. Sakuda, Y. Sato, A. Hayashi and M. Tatsumisago, *Energy Technol.*, 2019, **7**, 1900077.
157. H. Zhong, Y. Su, Y. Wu, J. Gu, R. Ma, Y. Luo, H. Lin, M. Tao, J. Chen, Z. Liang, K. Wang, X. Zheng, Z. Chen, J. Peng, Z. Lv, Z. Gong, J. Huang and Y. Yang, *Adv. Energy Mater.*, 2023, **13**, 2300767.
158. C. Y. Kwok, S. Xu, I. Kochetkov, L. Zhou and L. F. Nazar, *Energy Environ. Sci.*, 2023, **16**, 610-618.
159. X. Gao, X. Zheng, Y. Tsao, P. Zhang, X. Xiao, Y. Ye, J. Li, Y. Yang, R. Xu, Z. Bao and Y. Cui, *J. Am. Chem. Soc.*, 2021, **143**, 18188-18195.
160. H. Kim, H.-N. Choi, J.-Y. Hwang, C. S. Yoon and Y.-K. Sun, *ACS Energy Lett.*, 2023, **8**, 3971-3979.
161. Z. Zhang, B. Zhao, S. Zhang, J. Zhang, P. Han, X. Wang, F. Ma, D. Sun, Y. Jin, K. Kanamura and G. Cui, *J. Power Sources*, 2021, **487**, 229428.
162. Z. Chen, Z. Liang, H. Zhong, Y. Su, K. Wang and Y. Yang, *ACS Energy Lett.*, 2022, **7**, 2761-2770.
163. C. Duan, Z. Cheng, W. Li, F. Li, H. Liu, J. Yang, G. Hou, P. He and H. Zhou, *Energy Environ. Sci.*, 2022, **15**, 3236-3245.
164. J. Li, H. Zhang, Y. Cui, H. Da, H. Wu, Y. Cai and S. Zhang, *Chem. Eng. J.*, 2023, **454**, 140385.
165. H. Yuan, H.-X. Nan, C.-Z. Zhao, G.-L. Zhu, Y. Lu, X.-B. Cheng, Q.-B. Liu, C.-X. He, J.-Q. Huang and Q. Zhang, *Batteries Supercaps*, 2020, **3**, 596-603.
166. M. Fiedler, S. Cangaz, F. Hippauf, S. Dörfler, T. Abendroth, H. Althues and S. Kaskel, *Adv. Sustain. Syst.*, 2023, **7**, 2200439.
167. R.-c. Xu, X.-h. Xia, X.-l. Wang, Y. Xia and J.-p. Tu, *J. Mater. Chem. A*, 2017, **5**, 2829-2834.
168. N. Ahmad, L. Zhou, M. Faheem, M. K. Tufail, L. Yang, R. Chen, Y. Zhou and W. Yang, *ACS Appl. Mater. Interfaces*, 2020, **12**, 21548-21558.
169. M. K. Tufail, L. Zhou, N. Ahmad, R. Chen, M. Faheem, L. Yang and W. Yang, *Chem. Eng. J.*, 2021, **407**, 127149.
170. L. Zhou, M. K. Tufail, N. Ahmad, T. Song, R. Chen and W. Yang, *ACS Appl. Mater. Interfaces*, 2021, **13**, 28270-28280.
171. Z. Wu, S. Chen, C. Yu, C. Wei, L. Peng, H.-L. Wang, S. Cheng and J. Xie, *Chem. Eng. J.*, 2022, **442**, 136346.
172. C. Wei, C. Yu, L. Peng, Z. Zhang, R. Xu, Z. Wu, C. Liao, W. Zhang, L. Zhang, S. Cheng and J. Xie, *Mater. Adv.*, 2022, **3**, 1047-1054.
173. B.-S. Zhao, L. Wang, P. Chen, S. Liu, G.-R. Li, N. Xu, M.-T. Wu and X.-P. Gao, *ACS Appl. Mater. Interfaces*, 2021, **13**, 34477-34485.
174. W. Zhang, Y. Zhang, L. Peng, S. Li, X. Wang, S. Cheng and J. Xie, *Nano Energy*, 2020, **76**, 105083.
175. Q. Wang, Y. Chen, J. Jin and Z. Wen, *Solid State Ion.*, 2020, **357**, 115500.
176. P.-F. Wang, Y.-H. Zhao, S.-H. Tian, Z. Shen and T.-F. Yi, *Energy Fuels*, 2023, **37**, 15198-15205.
177. H. Zhang, U. Oteo, X. Judez, G. G. Eshetu, M. Martinez-Ibañez, J. Carrasco, C. Li and M. Armand, *Joule*, 2019, **3**, 1689-1702.
178. C. Yu, S. Ganapathy, E. R. H. v. Eck, H. Wang, S. Basak, Z. Li and M. Wagemaker, *Nat. Commun.*, 2017, **8**, 1086.
179. W. Pan, K. Yamamoto, T. Matsunaga, T. Watanabe, M. Kumar, N. Thakur, T. Uchiyama, M. Uesugi, A. Takeuchi, A. Sakuda, A. Hayashi, M. Tatsumisago, and Y. Uchimoto, *Batteries & Supercaps*, 2024, **9**, e202300427.
180. J. Zhou, M. L. H. Chandrappa, S. Tan, S. Wang, C. Wu, H. Nguyen, C. Wang, H. Liu, S. Yu, Q. R. S. Miller, G. Hyun, J. Holoubek, J. Hong, Y. Xiao, C. Soulen, Z. Fan, E. E. Fullerton, C. J. Brooks, C. Wang, R. J. Clément, Y. Yao, E. Hu, S. P. Ong, and P. Liu, *Nature*, 2024, **627**, 301-305.
181. M. Nagao, A. Hayashi and M. Tatsumisago, *Energy Technol.*, 2013, **1**, 186-192.
182. A. Kızılaslan, Ş. Efe and H. Akbulut, *J. Solid State Electrochem.*, 2020, **24**, 2279-2288.
183. Q. Zhang, N. Huang, Z. Huang, L. Cai, J. Wu and X. Yao, *J. Energy Chem.*, 2020, **40**, 151-155.
184. L.-P. Hou, H. Yuan, C.-Z. Zhao, L. Xu, G.-L. Zhu, H.-X. Nan, X.-B. Cheng, Q.-B. Liu, C.-X. He, J.-Q. Huang and Q. Zhang, *Energy Storage Mater.*, 2020, **25**, 436-442.

185. K. Suzuki, M. Tateishi, M. Nagao, Y. Imade, T. Yokoi, M. Hirayama, T. Tatsumi and R. Kanno, *J. Electrochem. Soc.*, 2017, **164**, A6178.
186. T. Ando, Y. Sato, T. Matsuyama, A. Sakuda, M. Tatsumisago and A. Hayashi, *J. Ceram. Soc. Jpn.*, 2020, **128**, 233-237.
187. G. Xu, Z. Yan, H. Yang, X. Zhang, Y. Su, Z. Huang, L. Zhang, Y. Tang, Z. Wang, L. Zhu, J. Lin, L. Yang and J. Huang, *Small*, 2023, **19**, 2300420.
188. X. Sun, Q. Li, D. Cao, Y. Wang, A. Anderson and H. Zhu, *Small*, 2022, **18**, e2105678.
189. Y. Zhang, T. Liu, Q. Zhang, X. Zhang, S. Wang, X. Wang, L. Li, L.-Z. Fan, C.-W. Nan and Y. Shen, *J. Mater. Chem. A*, 2018, **6**, 23345-23356.
190. C. Wang, Y. Wu, J. Gao, X. Sun, Q. Zhao, W. Si, Y. Zhang, K. Wang, F. Zhao, T. Ohsaka, F. Matsumoto, C. Huang and J. Wu, *ACS Appl. Mater. Interfaces*, 2023, **15**, 40496-40507.
191. L. Wang, X. Yin, B. Li and G. W. Zheng, *Nano Lett.*, 2022, **22**, 433-440.
192. C. Zhao, G.-L. Xu, Z. Yu, L. Zhang, I. Hwang, Y.-X. Mo, Y. Ren, L. Cheng, C.-J. Sun, Y. Ren, X. Zuo, J.-T. Li, S.-G. Sun, K. Amine and T. Zhao, *Nat. Nanotech.*, 2021, **16**, 166-173.
193. X. Sun, D. Cao, Y. Wang, T. Ji, W. Liang and H. Zhu, *Adv. Mater. Interfaces*, 2022, **9**, 2200539.
194. X. Meng, Y. Liu, Y. Ma, Y. Boyjoo, J. Liu, J. Qiu and Z. Wang, *Adv. Mater.*, 2023, **35**, 2212039.
195. S. Xu, C. Y. Kwok, L. Zhou, Z. Zhang, I. Kochetkov and L. F. Nazar, *Adv. Funct. Mater.*, 2021, **31**, 2004239.
196. K. Hikima, R. Fujii, H. Gamo, H. Tsukasaki, S. Mori, T. Watanabe, K. Yamamoto, Y. Uchimoto, H. Muto and A. Matsuda, *J. Phys. Chem. C*, 2023, **127**, 13511-13517.
197. N. H. H. Phuc, M. Takaki, M. Hiroyuki and M. Atsunori, *Front. Energy Res.*, 2021, **8**.
198. J. P. Mwizerwa, Q. Zhang, F. Han, H. Wan, L. Cai, C. Wang and X. Yao, *ACS Appl. Mater. Interfaces*, 2020, **12**, 18519-18525.
199. S. M. Hosseini, A. Varzi, S. Ito, Y. Aihara and S. Passerini, *Energy Storage Mater.*, 2020, **27**, 61-68.
200. H. U. Choi, J. S. Jin, J.-Y. Park and H.-T. Lim, *J. Alloys Compd.*, 2017, **723**, 787-794.
201. M. Iwao, H. Miyamoto, H. Nakamura, E. Hayakawa, S. Ohsaki and S. Watano, *Adv. Energy Sustain. Res.*, 2023, **n/a**, 2200206.
202. J. Yue, Y. Huang, S. Liu, J. Chen, F. Han and C. Wang, *ACS Appl. Mater. Interfaces*, 2020, **12**, 36066-36071.
203. C. Yan, Y. Zhou, H. Cheng, R. Orenstein, P. Zhu, O. Yildiz, P. Bradford, J. Jur, N. Wu, M. Dirican and X. Zhang, *Energy Storage Mater.*, 2022, **44**, 136-144.
204. L. Wang, X. Yin, C. Jin, C. Lai, G. Qu and G. W. Zheng, *ACS Appl. Energy Mater.*, 2020, **3**, 11540-11547.
205. W. Li, Q. Wang, J. Jin, Y. Li, M. Wu and Z. Wen, *Energy Storage Mater.*, 2019, **23**, 299-305.
206. Y. Liu, H. Liu, Y. Lin, Y. Zhao, H. Yuan, Y. Su, J. Zhang, S. Ren, H. Fan and Y. Zhang, *Adv. Funct. Mater.*, 2021, **31**, 2104863.
207. I. Garbayo, A. Santiago, X. Judez, A. S. de Buruaga, J. Castillo and M. A. Muñoz-Márquez, *ACS Appl. Energy Mater.*, 2021, **4**, 2463-2470.
208. Z. Lin, O. Sheng, X. Cai, D. Duan, K. Yue, J. Nai, Y. Wang, T. Liu, X. Tao and Y. Liu, *J. Energy Chem.*, 2023, **81**, 358-378.
209. P. P. Paul, B.-R. Chen, S. A. Langevin, E. J. Dufek, J. Nelson Weker and J. S. Ko, *Energy Storage Mater.*, 2022, **45**, 969-1001.
210. Z. Wang, J. Xia, X. Ji, Y. Liu, J. Zhang, X. He, W. Zhang, H. Wan and C. Wang, *Nat. Energy*, 2024, DOI: 10.1038/s41560-023-01426-1.
211. L. Ye, Y. Lu, Y. Wang, J. Li and X. Li, *Nat. Mater.*, 2024, DOI: 10.1038/s41563-023-01722-x.
212. H. Wan, Z. Wang, W. Zhang, X. He and C. Wang, *Nature*, 2023, **623**, 739-744.
213. A. Kızılaslan, T. Çetinkaya and H. Akbulut, *Adv. Mater. Interfaces*, 2020, **7**, 2001020.
214. H. Wan, Z. Wang, S. Liu, B. Zhang, X. He, W. Zhang and C. Wang, *Nat. Energy*, 2023, **8**, 473-481.
215. D. K. Singh, T. Fuchs, C. Krempaszky, B. Mogwitz, S. Burkhardt, F. H. Richter and J. Janek, *Adv. Funct. Mater.*, 2023, **33**, 2211067.
216. H. Wan, S. Liu, T. Deng, J. Xu, J. Zhang, X. He, X. Ji, X. Yao and C. Wang, *ACS Energy Lett.*, 2021, **6**, 862-868.
217. G. G. Eshetu, X. Judez, C. Li, O. Bondarchuk, L. M. Rodriguez-Martinez, H. Zhang and M. Armand, *Angew. Chem. Int. Ed.*, 2017, **56**, 15368-15372.
218. A. Santiago, J. Castillo, I. Garbayo, A. Saenz de Buruaga, J. A. Coca Clemente, L. Qiao, R. Cid Barreno, M. Martinez-Ibañez, M. Armand, H. Zhang and C. Li, *ACS Appl. Energy Mater.*, 2021, **4**, 4459-4464.
219. S. K. Kannan, J. Joseph and M. G. Joseph, *Energy Fuels*, 2023, **37**, 6302-6322.
220. M. Li, J. E. Frerichs, M. Kolek, W. Sun, D. Zhou, C. J. Huang, B. J. Hwang, M. R. Hansen, M. Winter and P. Bieker, *Adv. Funct. Mater.*, 2020, **30**, 1910123.
221. J.-K. Hu, H. Yuan, S.-J. Yang, Y. Lu, S. Sun, J. Liu, Y.-L. Liao, S. Li, C.-Z. Zhao and J.-Q. Huang, *J. Energy Chem.*, 2022, **71**, 612-618.
222. Z. Lv, J. Liu, C. Li, J. Peng, C. Zheng, X. Zheng, Y. Wu, M. Xia, H. Zhong, Z. Gong and Y. Yang, *eTransportation*, 2024, **19**, 100298.
223. X. Zhu, W. Jiang, L. Wang, and J. Lu, *Adv. Energy Mater.*, 2024, 234244.
224. H. Liu, Y. Liang, C. Wang, D. Li, X. Yan, C.-W. Nan and L.-Z. Fan, *Adv. Mater.*, 2022, **35**, 2206013.
225. A. Miura, N. C. Rosero-Navarro, A. Sakuda, K. Tadanaga, N. H. H. Phuc, A. Matsuda, N. Machida, A. Hayashi and M. Tatsumisago, *Nat. Rev. Chem.*, 2019, **3**, 189-198.
226. S.-H. Hwang, S.-D. Seo and D.-W. Kim, *Adv. Sci.*, 2023, **10**, 2301707.
227. Z. D. Hood, A. U. Mane, A. Sundar, S. Tepavcevic, P. Zapol, U. D. Eze, S. P. Adhikari, E. Lee, G. E. Sterbinsky, J. W. Elam and J. G. Connell, *Adv. Mater.*, 2023, **35**, 2300673.
228. J. Lee, T. Lee, K. Char, K. J. Kim and J. W. Choi, *Acc. Chem. Res.*, 2021, **54**, 3390-3402.
229. C. Wang, W. Ping, Q. Bai, H. Cui, R. Hensleigh, R. Wang, A. H. Brozena, Z. Xu, J. Dai, Y. Pei, C. Zheng, G. Pastel, J. Gao, X. Wang, H. Wang, J.-C. Zhao, B. Yang, X. Zheng, J. Luo, Y. Mo, B. Dunn and L. Hu, *Science*, 2020, **368**, 521-526.
230. W. Zaman and K. B. Hatzell, *Curr. Opin. Solid State Mater. Sci.*, 2022, **26**, 101003.

231. J. Schnell, F. Tietz, C. Singer, A. Hofer, N. Billot and G. Reinhart, *Energy Environ. Sci.*, 2019, **12**, 1818-1833.
232. A. Chen, C. Qu, Y. Shi and F. Shi, *Front. Energy Res.*, 2020, **8**.
233. D. Cao, Y. Zhao, X. Sun, A. Natan, Y. Wang, P. Xiang, W. Wang and H. Zhu, *ACS Energy Lett.*, 2020, **5**, 3468-3489.
234. X. Yang, K. R. Adair, X. Gao and X. Sun, *Energy Environ. Sci.*, 2021, **14**, 643-671.
235. J. Wu, L. Yuan, W. Zhang, Z. Li, X. Xie and Y. Huang, *Energy Environ. Sci.*, 2021, **14**, 12-36.
236. M. Batzer, C. Heck, P. Michalowski and A. Kwade, *Batteries Supercaps*, 2022, **5**, e202200328.
237. C. Singer, J. Schnell and G. Reinhart, *Energy Technol.*, 2021, **9**, 2000665.
238. L.-Z. Fan, H. He and C.-W. Nan, *Nat. Rev. Mater.*, 2021, **6**, 1003-1019.
239. K.-N. Jung, H.-S. Shin, M.-S. Park and J.-W. Lee, *ChemElectroChem*, 2019, **6**, 3842-3859.
240. J. Schnell, H. Knörzer, A. J. Imbsweiler and G. Reinhart, *Energy Technol.*, 2020, **8**, 1901237.
241. J. Schnell, T. Günther, T. Knoche, C. Vieider, L. Köhler, A. Just, M. Keller, S. Passerini and G. Reinhart, *J. Power Sources*, 2018, **382**, 160-175.
242. L. Xu, Y. Lu, C.-Z. Zhao, H. Yuan, G.-L. Zhu, L.-P. Hou, Q. Zhang and J.-Q. Huang, *Adv. Energy Mater.*, 2021, **11**, 2002360.
243. Topspeed, 10 Automakers Deeply Invested In Solid State Batteries, https://www.topspeed.com/automakers-invested-in-solid-state-batteries, (accessed December 2, 2023).
244. R. Deng, M. Wang, H. Yu, S. Luo, J. Li, F. Chu, B. Liu and F. Wu, *Energy Environ. Mater.*, 2022, **5**, 777-799.
245. Z. Han, R. Gao, Y. Jia, M. Zhang, Z. Lao, B. Chen, Q. Zhang, C. Li, W. Lv and G. Zhou, *Mater. Today*, 2022, **57**, 84-120.
246. S. Dörfler, S. Walus, J. Locke, A. Fotouhi, D. J. Auger, N. Shateri, T. Abendroth, P. Härtel, H. Althues and S. Kaskel, *Energy Technol.*, 2021, **9**, 2000694.
247. Y.-T. Liu, S. Liu, G.-R. Li and X.-P. Gao, *Adv. Mater.*, 2021, **33**, 2003955.
248. S. Xia, X. Wu, Z. Zhang, Y. Cui and W. Liu, *Chem*, 2019, **5**, 753-785.
249. G. Li, Z. Chen and J. Lu, *Chem*, 2018, **4**, 3-7.
250. NASA, NASA's Solid-State Battery Research Exceeds Initial Goals, Draws Interest, https://www.nasa.gov/aeronautics/nasas-solid-state-battery-research-exceeds-initial-goals-draws-interest, (accessed December 2, 2023).
251. United States Council For Automotive Research (USCAR), Goals for Advanced High-Performance Batteries for Electric Vehicle (EV) Applications, https://uscar.org/usabc, (accessed Mar 3, 2024).
252. ARPA-E, U.S. Department of Energy Announces $30 Million to Develop High-Energy Storage Solutions to Electrify Domestic Aircraft, Railroads & Ships, https://arpa-e.energy.gov/news-and-media/press-releases/us-department-energy-announces-30-million-develop-high-energy-storage, (accessed Mar 3, 2024).